Spring 5-18-2018

Active Vibration Control of Helicopter Rotor Blade by Using a Linear Quadratic Regulator

Md Mosleh Uddin
muddin2@uno.edu

Active Vibration Control of a Helicopter Rotor Blade by Using a Linear Quadratic Regulator

A Thesis

Submitted to the Graduate Faculty of the
University of New Orleans
in partial fulfillment of the

Master of Science
in
Engineering - Mechanical concentration

by

Md Mosleh Uddin

B.Sc., Islamic University of Technology, 2011
M.Sc., Technical University of Munich, 2015

May, 2018

Dedication

To

My Parents

without whose motivation, I couldn't have embarked on the journey of my higher studies

and

My Wife

whose presence inspire me to face any struggle on the way to achieve my dream

Acknowledgement

I am grateful to almighty God for encompassing me with his mercy and blessings beyond my expectations. I thank him for enabling me to pursue this research and to write this thesis after the successful completion of the project which is one of the best achievements in my life.

I would like to express my gratitude to my advisor, Dr. Uttam K. Chakravarty for giving me the opportunity to work in this challenging project. Without his guidance and continuous motivation, I wouldn't be able to conduct this research in which I had very little knowledge. I remember that frustrating moments when I planned to give up, but he inspired me and showed me the perfect way of solving challenging problems. I want to thank the members of my thesis committee; Dr. Paul J. Schilling and Dr. Martin J. Guillot for their valuable comments on my research.

I heartily thank my project member Pratik Sarker from whom I have learned valuable theoretical and practical aspects of my research for the last two years. I especially thank my fellow lab mate M Shafiqur Rahman who was more than a friend to help me whenever I faced any hurdle. I wouldn't get an enjoyable time during my study at the University of New Orleans if Mohammad Khairul Habib Pulok and Iftekhar Alam Riyad were not around.

This research was supported by the NASA EPSCoR Research Infrastructure Development (RID) grant (Contract No. LEQSF-EPS (2015)-RAP-17).

Contents

Nomenclature

A_d	Rotor disk area
D	Drag force
D_{by}	Bending stiffness with respect to y-axis
D_{bz}	Bending stiffness with respect to z-axis
D_t	Torsional rigidity of the cross section
I	Identity matrix
K	State feedback controller gain matrix
L	Lift force
M	Torsional moment
M_x	Internal moment about x-axis
M_y	Internal moment about y-axis
M_z	Internal moment about z-axis
R	Radius of the rotor blade
T	Centrifugal tension due to the rotation of the blade
V_∞	Velocity of the helicopter
V_{tip}	Linear rotor tip velocity
V_y	Internal shear force along y-axis
V_z	Internal shear force along z-axis
c	Cord length of the rotor blade
c_d	Drag coefficient
c_l	Lift coefficient
c_m	Pitching moment coefficient
e	Distance between the shear center and centroid
e_1	Offset from the rotating axis
f_y	External force per unit length along y-axis
f_z	External force per unit length along z-axis
l	Length of the rotor blade

m_x	External moment per unit length about x-axis
u_t	Linear blade velocity
v	Deflections due to lead-lag along y-axis
w	Deflections due to flapping along z-axis
α	Blade twist angle
α_a	Angle of attack
ζ_n	Damping ratio
κ_m	Polar mass radius of gyration about the elastic axis
κ_{m1}	Mass radius of gyration about the neutral axis
κ_{m2}	Mass radius of gyration about an axis normal to the chord through the shear center
ω_n	Natural frequency of n^{th} mode
Ω	Angular velocity of the rotor blade in rad/s
θ	Rotational deflections due to torsion about x-axis
μ	Advance ratio
σ	Solidity of the helicopter rotor blade

List of Figures

List of Tables

Abstract

Active vibration control is a widely implemented method for the helicopter vibration control. Due to the significant progress in microelectronics, this technique outperforms the traditional passive control technique due to weight penalty and lack of adaptability for the changing flight conditions. In this thesis, an optimal controller is designed to attenuate the rotor blade vibration. The mathematical model of the triply coupled vibration of the rotating cantilever beam is used to develop the state-space model of an isolated rotor blade. The required natural frequencies are determined by the modified Galerkin method and only the principal aerodynamic forces acting on the structure are considered to obtain the elements of the input matrix. A linear quadratic regulator is designed to achieve the vibration reduction at the optimum level and the controller is tuned for the hovering and forward flight with different advance ratios.

Keywords: Helicopter vibration, Control, Linear quadratic regulator, Rotating beam

Chapter 1

Introduction

1.1 Motivation

Vibration is an unavoidable phenomenon in every dynamic system defined as the oscillatory motion of the system. Regardless of the nature of complexity, due to the inherent mass and relative motions of the parts of any system some oscillatory movements are produced. Vibration in the mechanical system is considered as the disturbance to the system resulting wastage of energy, reduction of the efficiency, and decrease of the life time. Vibrations are responsible for the failure in civil structures that may cause severe damages to resources and human life. In automotive or aerospace vehicles, vibration is the prime cause of reducing component life and associated acoustic noise that causes passenger discomfort. However, this vibratory motion is not always objectionable and necessary to perform a certain task by the machine parts. Therefore, vibration control has become a significant task for the design engineer for maximizing the performance of the machine. The main objective of vibration control is to remove the unwanted oscillatory motion either produced by the external disturbance or due to the internal imbalance of the structure. Although the field of vibration control was intensively explored for many decades, the selection of the control technique is still challenging to the engineers.

1.2 Vibration Control Techniques

Various techniques were widely investigated and implemented to facilitate vibration control mechanism. These techniques can be divided into two major categories such as the passive vibration control and the active vibration control.

1.2.1 Passive Vibration Control: The passive vibration control excludes the necessity of the external energy sources to diminish the unwanted vibration of any system. This technique includes mass addition, force reduction, isolation, tuning, damping etc. In the vibration isolation technique, the energy of vibration is dissipated by using mechanical connections before it reaches the item to be controlled. The structural modification is also a part of the passive control techniques where the objective is to modify the stiffness of the structure. This procedure adjusts the system's frequency away from the resonance. Mass tuning, using the vibration absorber and adding damping to the troublesome vibration modes are some of the widely implemented passive vibration control techniques.

1.2.2 Active Vibration Control: The active vibration control generates forces to oppose the forces responsible for the vibration. This control technique incorporates three main components such as the sensor, controller, and actuator. The sensors measure the vibration at the location where they are placed and transfer signal to the controller. In practice, a controller is a computer or electronic hardware device. Based on the control algorithm, controller intelligently uses the sensed signal and transfers control signal to the actuators that exert forces to the desired locations. Even though this requires external power sources, the advancement in microprocessor, sensors, and actuators outperformed all other vibration control technologies.

Designing of the active vibration control technique includes many steps to be implemented. A typical scenario is described below:

1. Analysis of the vibratory system to be controlled.
2. Development of the idealized mathematical model of the system either by finite element analysis or modal analysis.

3. Reduction of the model size and simplification for the better integration with the control algorithm.
4. Analysis of the system properties, dynamics, responses, and disturbances.
5. Decision about the type and number of sensors, actuators, and their optimized locations.
6. Observation of the effect of sensors and actuators on the overall system dynamics.
7. Specification of the performance objective.
8. Determination of the control algorithm and designing of the controller to achieve the performance objective.
9. Simulation of the designed controlled system and optimization of the controller parameters.
10. Implementation of the controller by using hardware and software to the real system.
11. Update the system model based on the experimental results.

The typical steps of designing active control system are depicted by the flow chart in Fig. 1.1 [1].

1.3 Vibration in the Helicopter

Helicopter industry has the challenge of intense vibration problem generated from the complex dynamics of the system. The usage of the helicopter for the civil purpose is still limited due to the harmful effect of vibration and vibration induced noise. Helicopter vibration causes passenger discomfort and annoyance as well as health hazards to the pilot. It also causes structural fatigue of the helicopter components and reduces the reliability of the electronic equipment on board. Most often vibration added difficulties to the control of the helicopter for the pilot. The failures of the mechanical components caused many helicopter crashes. These failures can be predicted in advance by analyzing the signature of the vibration at several locations of the

helicopter. While understanding the fact that helicopter vibration can never be fully eliminated, the analysis and control of the vibration are essential to minimize the harmful effects and ensure the safety of the operation.

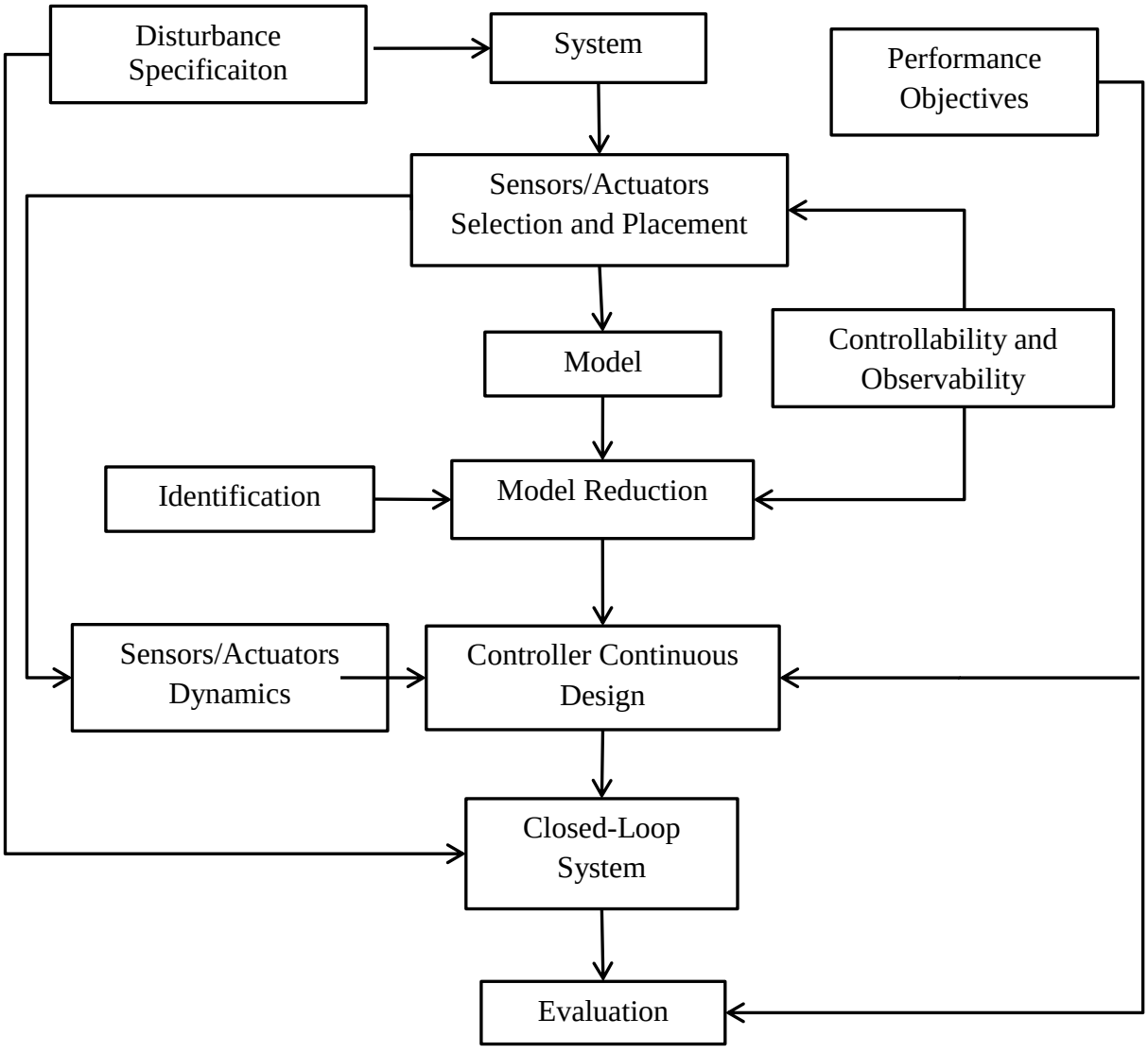

Figure 1.1: Flow chart of designing active vibration control technique

1.3.1 Sources of Vibration in the Helicopter: Among various sources of vibrations, main rotor hub forces and moments are the most contributing. The rotor blade experiences asymmetrical loading during the forward flight from the oscillatory air load that causes vibratory loads on the rotor assembly. During the forward flight, the velocity of airflow is larger on the advancing side compared to the retreating side. The resulting periodic variations of air loads produces periodic moments and forces at the blade root. Although most of the forces and moments are cancelled out while transferring to the fuselage frame, the remaining unbalanced forces and moments coalesce with the blade passing frequency $N\Omega$ (where N is the number of blade and Ω is the rotational speed of the rotor) [2].

Blade vortex interaction (BVI) is one of the major vibration sources, especially in the descending flight. When a blade passes the tip-vortices, shed by the previous blade, the impulsive load on the blade produces oscillatory movement to that blade. BVI is considered as the main source of noise generated by the helicopter. Another source of vibration can be the minor dissimilarities in the structural properties of the rotor blade. The unbalanced and misaligned moving parts generate harmonics and may produce structural resonance too. Although in modern manufacturing technologies this phenomenon is unlikely to happen, the defects in the materials can give raise this problem due to the long-term operation. The engine, gearbox, transmission, and tail rotor are also responsible for adding harmonics to the overall vibration. Depending on the helicopter model, the influence of the excitation may vary in a wider range.

1.3.2 Vibration Control Techniques in the Helicopter: There are several techniques available for the vibration reduction in the helicopter. From the application point of view, all the vibration control techniques are divided into several areas shown in Fig. 1.2.

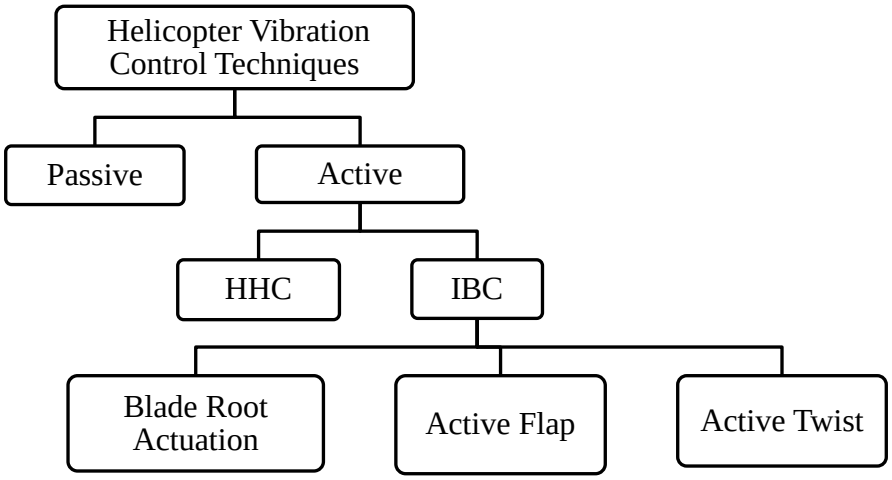

Figure 1.2: Vibration control techniques for the helicopter

1.3.2.1 Passive Control in the Helicopter: Passive vibration control is practically used for helicopter vibration control till recently, mostly with the use of vibration absorbers and vibration isolation system. Another approach is the optimization of the structural design to minimize the vibration of the helicopter. The main drawback of the passive system is the increase of drag when attached to rotating parts like rotor assembly. Additionally, this control system lacks the ability to adapt with the changing flight conditions such as speed, rotor rotational frequency, and structural dynamics due to different load conditions. Due to huge weight penalty and the inability to adapt with the transient flight conditions this method is not being implemented in the modern controller design [3].

1.3.2.2 Active Control in the Helicopter: To overcome the associated limitations in passive vibration control, active vibration control system is developed that can adapt to the changing flight conditions. Active control techniques are divided into two major categories with respect to the vibration attenuation location. The first technique is to reduce the generated

vibration at the rotor before the propagation into the fuselage and the second technique controls the vibration in the fuselage which is called as active control of structural response (ACSR). The recent vibration control approaches are mostly focused on reducing vibration at the rotor. Figure 1.3 shows the schematic diagram of the active vibration control technique in the helicopter. Active vibration control for the helicopter is divided into two major categories such as the higher harmonic control (HHC) and the individual blade control (IBC).

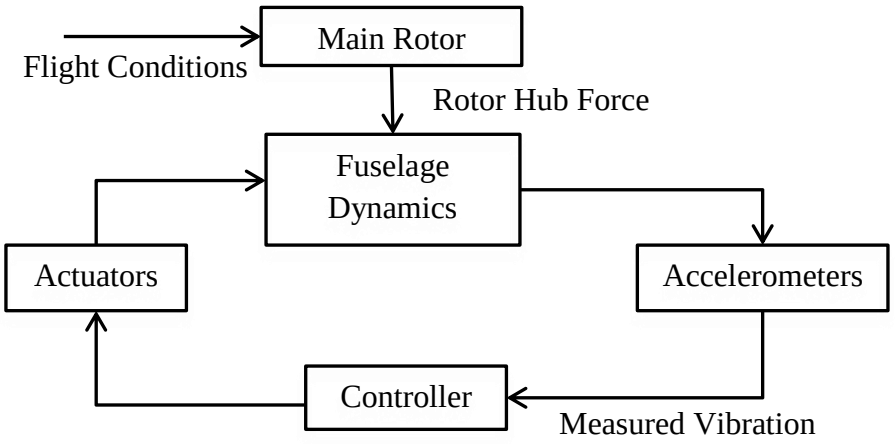

Figure 1.3: Schematic of active vibration control technique

Higher Harmonic Control (HHC): HHC is the widely analyzed and applied vibration control method where the rotor blades are actuated by additional hydraulic actuators attached to the nonrotating swash plate and accelerometers are placed at different fuselage locations [4]. HHC control is mostly considered in the recent research for the helicopter vibration control. The principal strategy is to add suitably phased harmonic components to the rotor controls to cancel the vibratory forces before or after the propagation into the fuselage [5, 6].

Individual Blade Control (IBC): Despite the simple implementation method of HHC, it has the limitation beyond some control frequencies which restricts the simultaneous noise and vibration control. In HHC, actuators are placed below the swash plate, therefore, the mechanically applicable control frequencies are limited to three blades [7]. IBC method is the most suitable method to overcome the limitations of the HHC. In the IBC, the actuators are attached to the rotating frame based on the same HHC algorithm. As each rotor blade is actuated individually, it also provides more flexibility to control undesirable dynamic phenomena. In the beginning, the application of the IBC started with the blade root actuation. The design was advanced with the emergence of the smart material which can be used as the actuator on the rotor blade for different vibration control mechanism such as the trailing edge flap, active twist along the rotor span, nose droop, and leading-edge flap [8]. The research and development of the IBC technology are yet to reach the level of the HHC and requires new manufacturing process of helicopter components for the practical implementation. Figure 1.4 shows the basic architecture of the HHC and the IBC control technique.

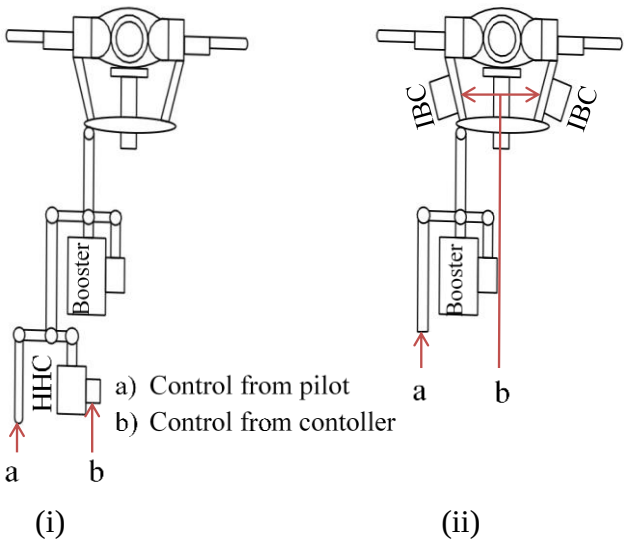

Figure 1.4: Basic architectures of (i) HHC and (ii) IBC

Different Types of IBC Technique:

Blade root actuation: Blade root actuation method is the most convenient method of IBC where the pitch links of the blades are replaced by the actuators that can control the pitch angle of each blade by reciprocating movement.

Active twist: Active twist actuation is the advanced way of IBC where no mechanical hinges or bearings are eliminated. The power of smart materials is used to generate the blade twist. The drawbacks of the active twist technique are the higher cost along with the weight penalty.

1.4 Literature Survey

The literature survey is done for the HHC and the IBC control separately. The focus is given to the IBC control and to each major category of this technique.

HHC Control: Johnson [9] provided a comprehensive review of the HHC algorithm and its variants along with the sequential history. HHC algorithms are categorized into three types based on the sharing properties. One type is the linear, quasi-static, frequency domain model of the helicopter response. The second type is the identification of a model, based on the least-squared error or the Kalman filter method. The third variant uses a quadratic cost function for control algorithm. From 1970 to late 1980, many experimental works on the rotor vibration control were reported based on the HHC algorithm. Shaw et al. [10] performed wind-tunnel test up to the advance ratio, $\mu = 0.3$ and showed that the vibratory hub loads were linearly dependent on the harmonic control input. Later, a closed-loop test was performed using the real-time identification of the transfer function. Three identification techniques were tested namely fixed gain controller, scheduled gain controller, and adaptive HHC controller. The fixed gain controller was proved to be the most successful vibration reduction technique reported by Shaw et al. [11]. This wind-tunnel

test was followed by the real flight test. HHC was tested in both the closed-loop and the open-loop on an OH-6A. Although the flight test showed a significant reduction in vibration, for the transient flight the results were not satisfactory [12]. Both the fixed gain and the adaptive controller showed satisfactory vibration reduction while tested on a SA349 Gazelle [13]. Through a series of numerical simulations by Hammond [14], Molusis [15], Nygrene and Schrage [16] by using the helicopter aeroelastic response code, the fixed gain controller was found to be the best identification technique. Jacklin [17] showed that both the least squares and the Kalman filter techniques gave comparable results where the Kalman filter technique required more parameter tuning. Closed-loop identification technique was found more difficult due to the low signal to noise ratio at minimum vibration level. A continuous time internal model, based on the non-adaptive variant of HHC was developed by Hall and Werely [18] which was identical to the classical *T*-matrix algorithm. Patt et al. [19] performed an analytic convergence and robustness analysis of the HHC from the control perspective. Mura et al. [4] proposed a noble algorithm to design a robust controller that integrates the model uncertainty due to the changing flight conditions. He adopted H_∞ approach that showed closed-loop performance similar to the linear quadratic (LQ) approach. The benefit was the reduced sensitivity to the feedback system uncertainty. A gain scheduling linear parameter varying (LPV) control law was also proposed by Mura et al. [20] as an alternative approach to the adaptive HHC control algorithm.

IBC Control:

Blade Root Actuation: Ham is considered as the pioneer of the IBC research at MIT who defined the IBC as the control method of each blade independently, having individual feedback loop built with the blade mounted sensors. Ham [21] performed analysis of IBC by using simple models by tuning feedback gain for one bladed model in the wind tunnel. He suggested that several

subsystems for controlling specific mode namely flapping, lagging, and torsion would make the IBC system more effective. He tested simple proportional feedback gain system for the closed-loop analysis and found 75% reduction in the bending response. Gust alleviation [22] and lead-lag damping [23] through the IBC was also investigated based on the mathematical equation of an isolated blade having flap and lag motion without any aerodynamic force. Simple proportional feedback along with a compensator was used for the analysis. Kessler et al. [24] performed a numerical study on an isolated rotor blade where flap, lag, and torsion were considered. At the moderate range of μ, lead-lag damping occurred moderately. Lead-lag damping was increased at the expense of large blade pitch amplitudes even for fixed gain, optimized for hovering condition. In 1993 and 1994, a full scale four bladed Bo 105 rotor with servo-hydraulic IBC was tested in the wind tunnel at the NASA Ames Center [25, 26]. The aim of this test was to reduce the vibration and BVI noise simultaneously along with the performance improvement.

A closed-loop IBC was explored for the vibration reduction by placing sensors on the rotating frame for input signal collection [27]. Based on a disturbance rejection type controller, 4/rev fuselage vibration was minimized by eliminating 4/rev hub force and moment excitation. The controller was designed in the time domain. By placing the strain gauges on the rotor hub and the shaft, flap bending moments were measured. The tested controller worked well at different flight phases and different speed ranges. Blade root actuation IBC system was tested on the 6-bladed CH-53G helicopter in a flight test [28, 29]. The test was conducted both in the open-loop phase and the closed-loop phase. For the open-loop phase by using 4/rev IBC, vibration reduction was significant, even for some sensor stations it was 100%. Based on the linear *T*- matrix, the control algorithm for the closed-loop test was developed. The objective was to reduce the vibration

at the selected accelerometer locations such as, at the main transmission and the cargo compartment. The reduction of the cost function was found 84%.

A full-scaled 4-bladed UH-60 rotor was tested at the Ames wind-tunnels in 2001 and 2009 [30]. The results of these two tests were outlined by Jacklin et al. [31] and Norman et al. [32]. The objective of these two tests was the performance improvement along with noise and vibration reduction. Although the instrumentations of these two tests were different, algorithms for both were linear *T*-matrix model. 3/rev frequency was found to be the most effective in reducing 4/rev vibrations.

The application and the performance of the blade root actuation method were proven successful in BVI noise reduction, vibration reduction, and performance improvement. However, for the blade root actuation method, hardware requirement is more intense resulting significant weight and cost penalties. To overcome the limitations of this method, smart actuation methods such as the active trailing edge flap and the active twist control are getting more attention nowadays.

Active Flap: At the NASA Ames wind-tunnel facility, a multi-cyclic twist control rotor was tested [33]. This four-bladed rotor used servo flaps aft of the trailing edge for controlling collective flap deflections. By using four electro-hydraulic flap actuators, this multi-cyclic control significantly reduces the blade bending moments. Millot et al. [26] investigated the vibration reduction by trailing edge flaps with aeroelastic simulation. A quadratic cost function consisting of the vibration and the control inputs was minimized for the controller design. Although the results were similar to the blade root actuation method, the power requirement of the blade root IBC was found eight times more than the active flap. Liu et al. [34] studied the performance enhancement

and the vibration reduction based on the single and dual flap mechanism. Their study was based on the simulation code for the model developed by Depailler and Friedmann [35] and adaptive control algorithm was applied. The single flap mechanism was proved superior to the dual flap by achieving 68% of the vibration reduction. The flight testing of the active trailing edge flap rotor was performed by Eurocopter in 2005 [36]. A BK 117 helicopter rotor was tested aiming to demonstrate the vibration and the noise reduction.

Active Twist: Active twist rotor blade was first investigated by Chopra [37] at the University of Maryland in 1993. Piezoceramic elements were embedded under the fiberglass skin of the blade at the top and the bottom surfaces. The tip twist amplitude was low due to high torsional stiffness. Two smart blades were manufactured in a joint project of Massachusetts Institute of Technology (MIT) and Penn State University [38]. Within the upper and the lower laminate of the blade spar, active fibers were placed. As the smart actuator was the embedded part of the blade structure, the design was less costly than the active flap. In a joint project of NASA, US Army, and MIT, a four-bladed articulated active twist rotor was tested in the heavy gas wind-tunnel [39]. At medium speed, significant vibration reduction was achieved whereas at high-speed vibration reduction was not satisfactory. Different types of the active rotor blade were manufactured and tested at Onera and DLR [40−42]. However, some issues need to be treated for the active twist actuator such as fatigue problem, maintenance, and repair facilities. A continuous trailing edge flap for primary flight control was studied where a bimorph designed with microfiber composite was used for the actuator. The initial testing results showed promising performance [43].

Hoffmann et al. [44] developed two experimental methods to improve the wind-tunnel-testing results for the active twist rotor with a developed rotor blade model. The discrepancies

between the actual structural properties of the rotor blade and the simulation model due to the instrumentation were reduced. Anobile et al. [45] showed the computational process for the synthesis of a low-frequency feedback controller aiming to alleviate the BVI noise. The noise emission sensitivity to the active twist actuation was investigated numerically, followed by the identification of the input-output variable for the closed-loop controller. Brillante et al. [46] compared two periodic control methods namely the optimal H_2 and the periodic static output feedback (POF) for the actively twisted rotor blade. The rotor blade of a Bo 105 helicopter was replaced with the macro fiber composite piezoelectric (MFCP) actuated blade and was simulated in a simple aerodynamic model.

1.5 Research Objective

Helicopter rotor blades undergo flapping, lead-lag, and torsional vibration due to the aerodynamic forces and structural couplings. The main objective of this thesis is to design a controller to attenuate the three degrees-of-freedom vibration of helicopter rotor blade. As discussed before, the helicopter is very complex in its dynamics hence requires a complex mathematical model to represent accurately. Due to the complex nature of the model, designing of the controller becomes laborious too. A comprehensive literature survey is performed to explore the concepts of the vibration control techniques in the helicopter field.

In this research, a mathematical model of the vibration of an isolated rotor blade of Bo 105 helicopter is derived. The equations of the coupled three degrees-of-freedom of vibration of the rotor blade are derived based on the analogy of a rotating cantilever beam. To maintain the simplicity of the model, only the principal aerodynamic forces such as lift, drag, and torsional moment are considered, and all other unsteady aerodynamic forces are neglected. The state-space

model of the coupled equations of motion is derived by using the separation of variable technique where the orthogonality conditions for the coupled equations of motion is utilized.

IBC technique is implemented to reduce the three degrees of vibration of the rotor blade. A linear quadratic regulator (LQR) is designed based on the derived state-space model using MATLAB control system toolbox. The controller is tuned in order to achieve the optimal vibration reduction for all degrees-of-freedom.

Chapter 2

Modeling of the Rotor Blade

2.1 Physical Model of the Helicopter Rotor Blade

A rotor system is the key component that helps the helicopter to maintain its unique dynamic characteristics of producing aerodynamic lift and thrust at the same time. The rotor system, in general, consists of two to five rotor blades connected to the hub. Based on how the rotor blades are attached to the hub, the rotor system can be classified into several categories. For this research, the rotor blade of Bo 105, a light-weight, multipurpose, twin engine helicopter, is used. The rotor blades of this helicopter are flexible and rigidly attached to the hub without any hinge. The major benefit of this blade is the reduction of the drag force experienced by the rotor blade. Unlike other counterparts, the hingeless rotor system, shown in Fig. 2.1, facilitates mechanical simplicity in the manufacturing and the maintenance. The rotor blades accommodate the aerodynamic forces by flexing and reduce the drag forces.

Figure 2.1: Hingeless rotor system

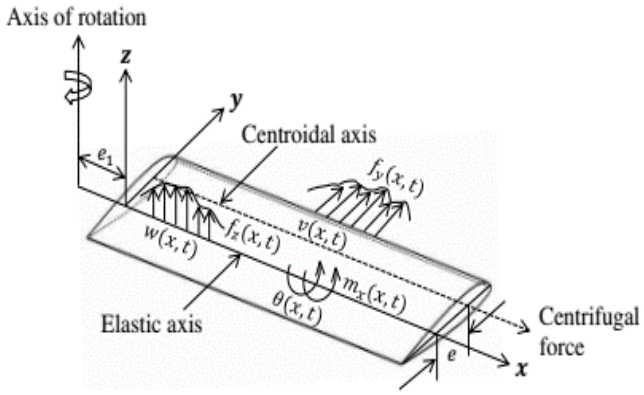

Figure 2.2: Geometry of the rotor blade

2.2 Properties of the Blade

The rotor blade of Bo 105 is manufactured of reinforced fiberglass plastic composite materials which increase the agility and the responsiveness of the helicopter. The blade is uniform from the root to the tip and can be considered as the cantilever beam having clamped-free boundary conditions. Table 1 provides different parameters of the main rotor system of the considered model that are necessary for the vibration analysis.

Table 1: Parameters of Bo 105 helicopter rotor system [47]

Parameters	**Value**	**Parameters**	**Value**
c	0.27 m	σ	0.07
l	4.22 m	Ω	44.50 rad/s
A_d	75.73 m^2	α	-8^o
V_{tip}	218.50 m/s	Airfoil profile	NACA 23012

2.3 Mathematical Modeling of the Helicopter Rotor Blade Vibration

The rotor blades of Bo 105 are bolted to the rotor hub resulting in the similar end condition of the cantilever beam [48]. The cross-section of this type of rotor blade is considered symmetric with respect to the principal centroidal axis. Sarker [49] considered the blade as Euler-Bernoulli beam subjected to out-of-plane displacement (flapping), in-plane displacement (lead-lag), and rotational displacement (torsion). Along the x-axis, all the rigidities are assumed constant.

The governing triply coupled equations of vibration for the Bo 105 helicopter rotor blade were written as [49],

$$
\begin{aligned}
&[D_{by}(x)w''(x,t) + D_{bzy}v''(x,t)]'' - [T(x)w'(x,t)]' \\
&-[\Omega^2 me(x+e_1)\theta(x,t)\,cos\alpha(x)]' + m[\ddot{w}(x,t) \\
&+e\ddot{\theta}(x,t)cos\alpha(x)] = f_z(x,t) + [\Omega^2 mexsin\alpha(x)]'
\end{aligned} \tag{1}
$$

$$
\begin{aligned}
&[D_{bz}(x)v''(x,t) + D_{bzy}w''(x,t)]'' - [T(x)v'(x,t)]' \\
&+[\Omega^2 me(x+e_1)\theta(x,t)sin\alpha(x)]' + \Omega^2 me\theta(x,t)sin\alpha(x) \\
&+m\left[\ddot{v}(x,t) - e\ddot{\theta}(x,t)sin\alpha(x)\right] - \Omega^2 mv(x,t) \\
&= f_y(x,t) + [\Omega^2 me(x+e_1)cos\alpha(x)]' + \Omega^2 mecos\alpha(x)
\end{aligned} \tag{2}
$$

$$
\begin{aligned}
&-[D_t(x)\theta'(x,t)]' - \Omega^2 me(x+e_1)[v'(x,t)sin\alpha(x) \\
&-w'(x,t)cos\alpha(x)] + \Omega^2 mev(x,t)sin\alpha(x) \\
&+\Omega^2 m\,cos\,2\alpha(x)\,(\kappa_{m2}^2 - \kappa_{m1}^2)\theta(x,t) + m\kappa_m^2\ddot{\theta}(x,t) \\
&-me[\ddot{v}(x,t)sin\alpha(x) - \ddot{w}(x,t)cos\alpha(x)] \\
&= m_x(x,t) - \Omega^2 m[(\kappa_{m2}^2 - \kappa_{m1}^2)sin\alpha(x)cos\alpha(x)]
\end{aligned} \tag{3}
$$

where "$'$" denotes the differentiation with respect to x, D_{by} and D_{bz} are the bending stiffness with respect to y-axis and z-axis shown in Fig. 2.2; D_t is the torsional rigidity; w, v, and θ are flapping, lead-lag, and torsional deflections, respectively; e_1 is the offset from the rotating axis; e is the distance between the shear center and the centroid; κ_m is the polar mass radius of gyration about the elastic axis; κ_{m1}, κ_{m2} are the mass radii of gyration about the neutral axis and the axis normal to chord through the shear center, respectively; f_z, f_y, and m_x are the aerodynamic lift, drag, and pitching moment per unit length, respectively; m is the mass per unit length; T is the centrifugal tension due to the rotation of the blade.

For the nonrotating case with $\alpha = 0$, Eqs. (1)−(3) become ($\Omega = 0$),

$$
D_{by}w'''' + m\ddot{w} + me\ddot{\theta} = f_z \tag{4}
$$

$$D_{bz}v'''' + m\ddot{v} = f_y \tag{5}$$

$$-D_t\theta'' + mk_m^2\ddot{\theta} + me\ddot{w} = m_x \tag{6}$$

Boundary Conditions:

The boundary conditions are similar to the clamped-free beam as follows,

At $x = 0$: $$w = v = \theta = w' = v' = \theta' = 0 \tag{7}$$

At $x = l$: $$M_y = M_z = V_y = V_z = 0 \tag{8}$$

where M_y and M_z denote the bending moments about the y and z axes, respectively; V_y and V_z denote the cross-sectional shear forces in y and z direction, respectively.

To obtain the time-varying deflections of the rotor blade, it is necessary to uncouple the equations of motion. The process of uncoupling the coupled equations of motion were described by Sarker [49]. Let the solution of the governing equations of motion are harmonic in nature with the following form:

$$w(x,t) = W_n(x)e^{i\omega_n t} \tag{9}$$

$$v(x,t) = V_n(x)e^{i\omega_n t} \tag{10}$$

$$\theta(x,t) = \Theta_n(x)e^{i\omega_n t} \tag{11}$$

By plugging Eqs. (9)−(11) into Eqs. (1)−(3) and considering the nonrotating case, free vibration equations of motion are (where $\alpha = 0$):

$$D_{by}W_n'''' - m\omega_n^2 W_n - me\omega_n^2\Theta_n = 0 \tag{12}$$

$$D_{bz}V_n'''' - m\omega_n^2 V_n = 0 \tag{13}$$

$$-D_t\Theta_n'' - m\omega_n^2\kappa_m^2\Theta_n - me\omega_n^2 W_n = 0 \tag{14}$$

Eqs. (12)−(14) can be rewritten as follows:

$$D_{by}W_n'''' - m\omega_n^2 W_n - me\omega_n^2\Theta_n = 0 \tag{15}$$

$$D_{bz}V_n'''' - m\omega_n^2 V_n = 0 \tag{16}$$

$$-D_t\Theta_n'' - m\omega_n^2\kappa_m^2\Theta_n - me\omega_n^2 W_n = 0 \tag{17}$$

Let

$$w(x,t) = \sum_{n=1}^{\infty} W_n(x)q_n(t) \tag{18}$$

$$v(x,t) = \sum_{n=1}^{\infty} V_n(x)q_n(t) \tag{19}$$

$$\theta(x,t) = \sum_{n=1}^{\infty} \Theta_n(x)q_n(t) \tag{20}$$

where W_n, V_n, and Θ_n are the flapping, lead-lag, and torsional mode shapes, respectively; q_n is the generalized time coordinate for the n^{th} mode of vibration.

Now the Eqs. (18)−(20) are plugged into Eqs. (4)−(6) and the resulting equations become,

$$\sum_{n=1}^{\infty} D_{by}W_n''''q_n + \sum_{n=1}^{\infty} mW_n\ddot{q_n} + \sum_{n=1}^{\infty} me\Theta_n\ddot{q_n} = f_z \tag{21}$$

$$\sum_{n=1}^{\infty} D_{bz}V_n''''q_n + \sum_{n=1}^{\infty} mV_n\ddot{q_n} = f_y \tag{22}$$

$$\sum_{n=1}^{\infty} -D_t\Theta_n''\, q_n + \sum_{n=1}^{\infty} m\kappa_m^2\Theta_n\ddot{q_n} + \sum_{n=1}^{\infty} meW_n\ddot{q_n} = m_x \tag{23}$$

Multiplying Eqs. (21)−(23) by W_m, V_m, and Θ_m, respectively and using the relations from Eqs. (15)−(17) and adding them together, the equation becomes,

$$\sum_{n=1}^{\infty}[(m\omega_n^2 W_n + me\omega_n^2\Theta_n)\,W_m q_n + mW_n W_m \ddot{q_n} + me\Theta_n W_m \ddot{q_n}$$
$$+m\omega_n^2 V_n V_m q_n + mV_n V_m \ddot{q_n} + (m\omega_n^2\kappa_m^2\Theta_n + me\omega_n^2 W_n)\Theta_m q_n$$
$$+m\kappa_m^2\Theta_n\Theta_m\ddot{q_n} + meW_n\Theta_m\ddot{q_n}] = f_z W_m + f_y V_m + m_x\Theta_m \quad (24)$$

The orthogonality relationship of the triply coupled vibration for the force vibration was derived by Sarker [49] as follows:

$$\int_0^l [W_m W_n + V_m V_n + e(W_m\Theta_n + W_n\Theta_m) + \kappa_m^2\Theta_m\Theta_n]dx = \delta_{mn} \quad (25)$$

where δ_{mn} is the Kronecker delta and is defined as,

$$\delta_{mn} = 1; \quad m = n \quad (26)$$

$$\delta_{mn} = 0; \quad m \neq n \quad (27)$$

By rearranging the terms in Eq. (24) and integrating from 0 to l , the equation is written as,

$$\sum_{n=1}^{\infty}\{m\ddot{q_n}\int_0^l [W_m W_n + V_m V_n + e(W_m\Theta_n + W_n\Theta_m) + \kappa_m^2\Theta_m\Theta_n]dx$$
$$+m\omega_n^2 q_n\int_0^l [W_m W_n + V_m V_n + e(W_m\Theta_n + W_n\Theta_m) + \kappa_m^2\Theta_m\Theta_n]dx\}$$
$$= \int_0^l \left(f_z W_n + f_y V_n + m_x\Theta_n\right)dx \quad (28)$$

By applying the orthogonality condition from Eq. (25) into Eq. (28), the following equation can be formed,

$$\ddot{q_n} + \omega_n^2 q_n = \frac{1}{m}\int_0^l \left(f_z W_n + f_y V_n + m_x \Theta_n\right) dx \tag{29}$$

$$\ddot{q}_n + \omega_n^2 q_n = F_z + F_y + M_x \tag{30}$$

Here,

$$F_z = \frac{1}{m}\int_0^l (f_z W_n) dx \tag{31}$$

$$F_y = \frac{1}{m}\int_0^l \left(f_y V_n\right) dx \tag{32}$$

$$M_x = \frac{1}{m}\int_0^l (m_x \Theta_n) dx \tag{33}$$

If damping is considered, then Eq. (30) can be derived as,

$$\ddot{q_n} + 2\,\zeta_n \omega_n \dot{q_n} + \omega_n^2 q_n = F_z + F_y + M_x \tag{34}$$

where ζ_n is the damping ratio of the n^{th} mode of vibration. For the rotating blade, the natural frequencies are replaced by the rotating natural frequencies, ω_{nr} and the equation becomes,

$$\ddot{q_n} + 2\,\zeta_n \omega_{nr} \dot{q_n} + \omega_{nr}^2 q_n = F_z + F_y + M_x \tag{35}$$

2.4 Forcing Functions

Helicopter rotor blades experience different types of loading for different operations such as hovering and forward flight. Although the types of these loading are not limited, for this thesis only the aerodynamic lift, drag, and the pitching moment are considered for the vibration analysis.

Hovering Case

The formula to calculate the aerodynamic forces for hovering are as follows [50]:

Lift force:

$$L(x) = \frac{1}{2}\rho_{air} u_t^2(x) c c_l(x) \tag{36}$$

Drag force:

$$D(x) = \frac{1}{2}\rho_{air} u_t^2(x) c c_d(x) \tag{37}$$

Pitching moment:

$$M(x) = \frac{1}{2}\rho_{air} u_t^2(x) c^2 c_m(x) \tag{38}$$

where ρ_{air} is the density of air, u_t is the linear blade velocity, c is the cord length, c_l, c_d, and c_m are lift, drag, and pitching moment coefficients, respectively.

The values of the aerodynamic coefficients are the function of the angle of attack, α and the Mach number. However, for the smaller value of α and subsonic Mach number, these coefficients can be calculated by the following formulas [50]:

Lift coefficient,

$$c_l = a\alpha_a \tag{39}$$

Drag coefficient,

$$c_d = d_0 + d_1\alpha_a + d_2\alpha_a^2 \tag{40}$$

Pitching moment coefficient,

$$c_m = m_0 + m_1\alpha_a \tag{41}$$

where a, d_0, d_1, d_2, m_0, and m_1 are the empirically derived coefficients for NACA 23012 airfoil with α_a as the angle of attack. The values are found in the literature: $a = 5.7$/rad, $d_0 = 0.0087$, $d_1 = -0.012$, $d_2 = 0.4$, and $c_m = -0.008$ [51].

Forward flight Case

For the forward flight case, the aerodynamic forces become the function of the azimuth angle, ψ also. The formulas [50] to calculate the aerodynamic forces are described below:

Lift force:

$$L = L(x,\psi) = \frac{1}{2}\rho_{air}u_t^2(x,\psi)cc_l(x,\psi) \tag{42}$$

Drag force:

$$D = D(x,\psi) = \frac{1}{2}\rho_{air}u_t^2(x,\psi)cc_d(x,\psi) \tag{43}$$

Pitching moment:

$$M = M(x,\psi) = \frac{1}{2}\rho_{air}u_t^2(x,\psi)c^2c_m(x,\psi) \tag{44}$$

In the forward flight, the linear blade velocity,

$$u_t = \Omega x + V_\infty sin\psi \tag{45}$$

where $\psi = \Omega t$, V_∞ is the velocity of the helicopter.

In the analysis of the helicopter dynamics, the advanced ratio (μ) is often considered for the measure of the forward velocity which is defined as the ratio of the freestream speed to the rotor tip speed.

$$\mu = \frac{V_\infty}{\Omega R} \tag{46}$$

where R is the radius of the rotor blade.

2.5 State-Space Model Development

In classical control theory, the multiple input, multiple output (MIMO) systems are expressed by the state-space equations to represent the dynamics of the system. The state-space model is important to analyze any dynamic system in the time domain.

The state-space equations of a dynamic system consist of the state vector, $\boldsymbol{x}$, control input vector, $\boldsymbol{u}$, and output vector, $\mathbf{y}$.

$$\dot{\boldsymbol{x}}(t) = A\boldsymbol{x}(t) + B\boldsymbol{u}(t) \tag{47}$$

$$\boldsymbol{y}(t) = C\boldsymbol{x}(t) + D\boldsymbol{u}(t) \tag{48}$$

where A, B, C, and D are time-invariant matrices.

In the following section, the state-space model for the rotor blade vibration is derived from Eq. (35).

For $n = 1$,

$$\ddot{q_1} + 2\,\zeta_1\omega_1\dot{q_1} + \omega_1^2 q_1 = F_z + F_y + M_x \tag{49}$$

$$\ddot{q_1} = -2\,\zeta_1\omega_1\dot{q_1} - \omega_1^2 q_1 + F_z + F_y + M_x \tag{50}$$

For $n = 2$,

$$\ddot{q_2} + 2\,\zeta_2\omega_2\dot{q_2} + \omega_2^2 q_2 = F_z + F_y + M_x \tag{51}$$

$$\ddot{q_2} = -2\,\zeta_2\omega_2\dot{q_2} - \omega_2^2 q_2 + F_z + F_y + M_x \tag{52}$$

For $n = 3$,

$$\ddot{q_3} + 2\,\zeta_3\omega_3\dot{q_3} + \omega_3^2 q_3 = F_z + F_y + M_x \tag{53}$$

$$\ddot{q_3} = -2\,\zeta_3\omega_3\dot{q_3} - \omega_3^2 q_3 + F_z + F_y + M_x \tag{54}$$

Let

$$x_1 = q_1(t) \tag{55}$$

$$x_2 = \dot{q}_1(t) = \dot{x}_1 \tag{56}$$

$$x_3 = q_2(t) \tag{57}$$

$$x_4 = \dot{q}_2(t) = \dot{x}_3 \tag{58}$$

$$x_5 = q_3(t) \tag{59}$$

$$x_6 = \dot{q}_3(t) = \dot{x}_5 \tag{60}$$

By considering the first mode of the flapping, lead-lag, and torsion, the states of the model can be expressed as follows,

$x_1 =$ tip displacement for flapping

$x_2 = \dot{x}_1 =$ derivative of the tip displacement for flapping

$x_3 =$ tip displacement for lead-lag

$x_4 = \dot{x}_3 =$ derivative of the tip displacement for lead-lag

$x_5 =$ tip displacement for torsion

$x_6 = \dot{x}_5 =$ derivative of the tip displacement for torsion

Based on the defined states, the state-space model takes the following form:

$$\begin{bmatrix}\dot{x}_1\\ \dot{x}_2\\ \dot{x}_3\\ \dot{x}_4\\ \dot{x}_5\\ \dot{x}_6\end{bmatrix}=\begin{bmatrix}0 & 1 & 0 & 0 & 0 & 0\\ -\omega_1^2 & -2\xi_1\omega_1 & 0 & 0 & 0 & 0\\ 0 & 0 & 0 & 1 & 0 & 0\\ 0 & 0 & -\omega_2^2 & -2\xi_2\omega_2 & 0 & 0\\ 0 & 0 & 0 & 0 & 0 & 1\\ 0 & 0 & 0 & 0 & -\omega_3^2 & -2\xi_3\omega_3\end{bmatrix}\begin{bmatrix}x_1\\ x_2\\ x_3\\ x_4\\ x_5\\ x_6\end{bmatrix}+\begin{bmatrix}0 & 0 & 0\\ F & 0 & 0\\ 0 & 0 & 0\\ 0 & F & 0\\ 0 & 0 & 0\\ 0 & 0 & F\end{bmatrix}u \quad (61)$$

$$F = F_z + F_y + M_x = \frac{1}{m}\int_0^l (f_z W_n + f_y V_n + m_x \Theta_n)\, dx \quad (62)$$

where ω_1, ω_2, and ω_3 are the flapping, lead-lag, and torsional natural frequencies of the 1st mode, respectively.

In this analysis, the desired outputs are the flapping, lead-lag, and torsional deflections at the blade tip. Therefore, the output equation becomes,

$$y = \begin{bmatrix}1 & 0 & 0 & 0 & 0 & 0\\ 0 & 0 & 1 & 0 & 0 & 0\\ 0 & 0 & 0 & 0 & 1 & 0\end{bmatrix}\begin{bmatrix}x_1\\ x_2\\ x_3\\ x_4\\ x_5\\ x_6\end{bmatrix} \quad (63)$$

Chapter 3

Controller Design

3.1 Types of Controller

The purpose of the controller is to eliminate the unwanted hub forces and moments by providing required control forces. The basic principle of any controller is to collect the measured data of the plant and to provide the control signal to the actuator based on the control algorithm. The selection of the proper control algorithm is the most important task for the control engineer. Control systems are mainly divided into two major categories such as feedback and feedforward control.

Feedback Control: Feedback control system measures the system states or outputs continuously. Based on the deviation of the outputs from the reference states, control signals are generated by the controller. This type of controller is suitable for modifying any dynamic behavior of the system. In the presence of uncertainty, the performance of this controller is high. The main drawback of this type of controller is the delayed response that may lead to instability.

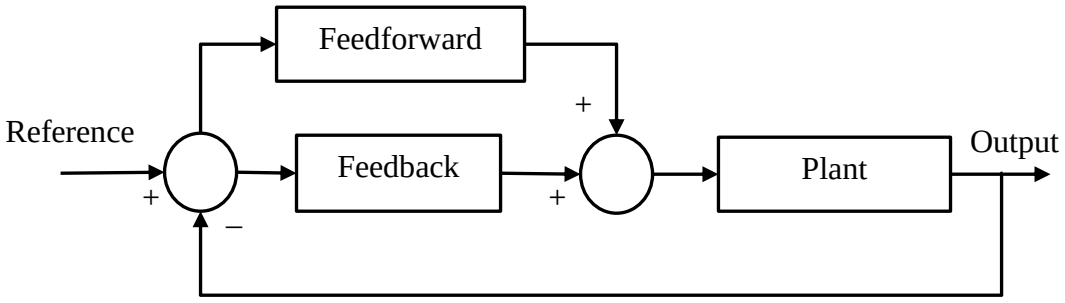

Figure 3.1: Schematic of the feedforward and feedback controller

Feedforward Control: Feedforward controller produces predefined control signal for the actuator, based on the system model. This controller is suitable to overcome the sluggish dynamics and delays while maintaining the stability. The system response must be predictable to implement this type of controller. When the effect of any disturbance is not predictable or any change in the system occurs, feedforward controllers are not applicable. Sometimes feedback and feedforward controllers are implemented together to achieve better performance.

3.2 Optimal Control Theory

In the modern feedback control, optimal control theory is the commonly used approach. Optimal control is the process of defining a control law to achieve a certain performance goal. A cost function consisting of the states and the control variables are optimized to minimize the cost function. For controlling any dynamic system, where the change of the state variables is not uniform, the optimal control theory is applicable. The optimal controller is suitable for the time domain analysis in the form of state-space model. The applications of the optimal controller for the MIMO models demand huge matrix operations. However, with the improvement of the digital computer and the microprocessor, the implementation costs are highly reduced.

3.2.1 LQR Controller Design

For the design of an optimal controller, the LQR based on state feedback is widely implemented [52]. This is an alternative approach to the direct pole placement technique where the best pole locations are implicitly chosen based on the LQ algorithm. Based on the derived state-space model, the optimal control law is implemented to determine the best feedback control gain matrix to reduce the vibration of the considered rotor blade. Figure 3.2 represents the block diagram of the LQR algorithm.

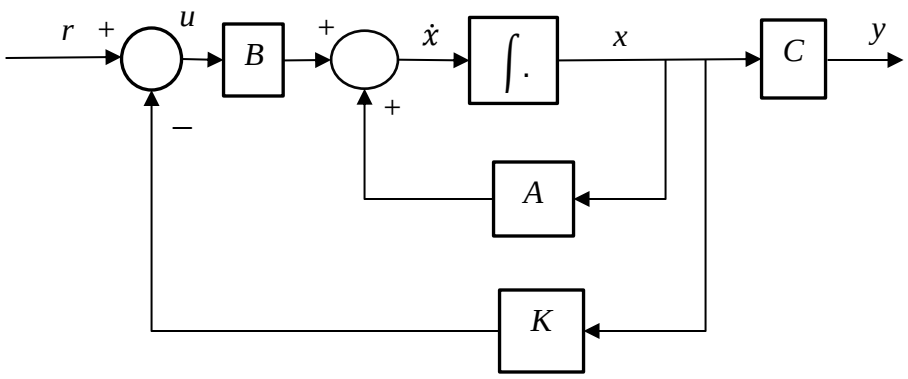

Figure 3.2: Block diagram of the LQR controller

In the regulator problem, the reference, r is considered zero. The state feedback control law, therefore, is defined as,

$$\boldsymbol{u}(t) = -K\boldsymbol{x}(t) \tag{64}$$

for the system dynamics defined by,

$$\dot{\boldsymbol{x}}(t) = A\boldsymbol{x}(t) + B\boldsymbol{u}(t) \tag{65}$$

With the controller, the closed-loop system dynamics becomes,

$$\dot{\boldsymbol{x}}(t) = (A - BK)\boldsymbol{x}(t) \tag{66}$$

where K is the state feedback controller gain matrix.

A quadratic cost function J is defined to be minimized by optimizing between control effort and control errors. Control errors are defined by the squared values of the state variables and the control efforts are described by the squared values of the control input. To minimize the control errors, more control effort is required, whereas the reduction of control effort increases the control errors. In LQR problem, the target is to find an input signal $\boldsymbol{u}(t)$ such that the cost function is minimized.

By introducing the relative cost with two parameter matrices Q and R, these two contradictory objectives are quantified as follows,

$$J = \frac{1}{2}\int_0^\infty [\boldsymbol{x}^T(t)Q\boldsymbol{x}(t) + \boldsymbol{u}^T(t)R\boldsymbol{u}(t)]dt \tag{67}$$

where Q and R are the positive semidefinite weighting matrices that need to be optimized. The relative values of Q and R define the importance on the state variables and the controller effort, not their absolute values. Therefore, the value of R can be kept as an identity matrix while varying the matrix Q. After determining the optimal value of R, the value of K will be found from,

$$K = R^{-1}B^TP \tag{68}$$

and P will be calculated by solving the algebraic Riccati equation,

$$PA + A^TP + C^TC - PBR^{-1}B^TP = 0 \tag{69}$$

For realizing the LQR controller, several assumptions are necessary. Such as,

a) Matrix (A, B) must be stabilizable and detectable [Stabilizable: All unstable modes are controllable; Detectable: All unstable modes are observable].
b) The solution for the matrix P is always symmetric.

Advantages of LQR Controller: This type of controller are preferred for the modern controller design to the classical controller as it offers several benefits from the design perspective. Such as,

a) The LQR controller provides stability of the plant if all the states are available to be measured.
b) The optimization of the controller requires tuning of few parameters.

Controllability: Controllability is an important property of the plant for the controller design. If a system can be transferred from an initial state to the final state in a finite time interval by certain input, the system is called controllable. A system is controllable if the controllability matrix is full rank, where rank is the number of the linearly independent rows (or columns). Controllability matrix Con is formed as follows,

$$Con = [B\ AB\ A^2B\ \ldots A^{n-1}B] \tag{70}$$

The controllability matrix can be easily constructed by the MATLAB command, $Con = ctrb(A, B)$ and the rank of the controllability matrix can be calculated by, $rank(Con)$.

The system matrix of the rotor blade has all of the eigenvalues in the left half plane (LHP). As there is no unstable mode, the system is fully stabilizable.

Chapter 4

Results and Discussion

4.1. Controlled Vibration Results

The derived state-space model is simulated to analyze the forced vibration for the forcing functions, mentioned in Chapter 3. For this research, only the first modes of the flapping, lead-lag, and torsional deflections are considered. To determine the elements of the input matrix, the forcing functions are multiplied with the corresponding mass normalized mode shapes. The natural frequencies of the first modes of flapping, lead-lag, and torsion are calculated by using the modified Galerkin method [49].

Table 2: The coupled natural frequencies of the rotor blade

Mode of Vibration	**Natural Frequency**
Flapping (1^{st} mode)	60 rad/s
Lead-lag (1^{st} mode)	48 rad/s
Torsion (1^{st} mode)	225 rad/s

For the simulation, 10% of the total lift, drag, and torsional moment are considered responsible for the vibration of the rotor blade. The damping of the rotor blade is the sum of the structural and the aerodynamic damping. However, the aerodynamic damping is significantly higher in flapping than the lead-lag and torsional cases. 20% damping ratio is considered for the flapping (according to Leishman [53]), whereas 2% damping ratio is considered for other cases.

4.2 Simulation Results for the Hovering Flight

Case 1: Sinusoidal Excitation Load

Figures 4.1–4.3 show the steady state flapping, lead-lag, and torsional deflections of the rotor blade tip for the lift, drag, and torsional moment, respectively. The lead-lag deflections are considered uncoupled from the flapping and the torsion as discussed in Chapter 2. To excite the state-space model, sinusoidal forces are applied as input. The controlled deflections are also depicted in the same plot for all three cases. The LQR controller is tuned in order to obtain the desired controlled deflections by varying the weighting matrix Q while assuming $R = I$. For all the cases, observations are shown for two different weighting matrices.

Figure 4.1 shows that for the flapping motion, the deflections of the blade tip fluctuate between -0.02 m and 0.02 m and the nature is sinusoidal due to similar nature of the input force. The controlled defection is also shown for the weighting matrix $Q = 200I$ in Fig. 4.1 (a) and $Q = 500I$ in Fig. 4.1 (b). The increase of the Q value decreases the controlled deflections. However, the improvement is not significant with respect to the controller effort.

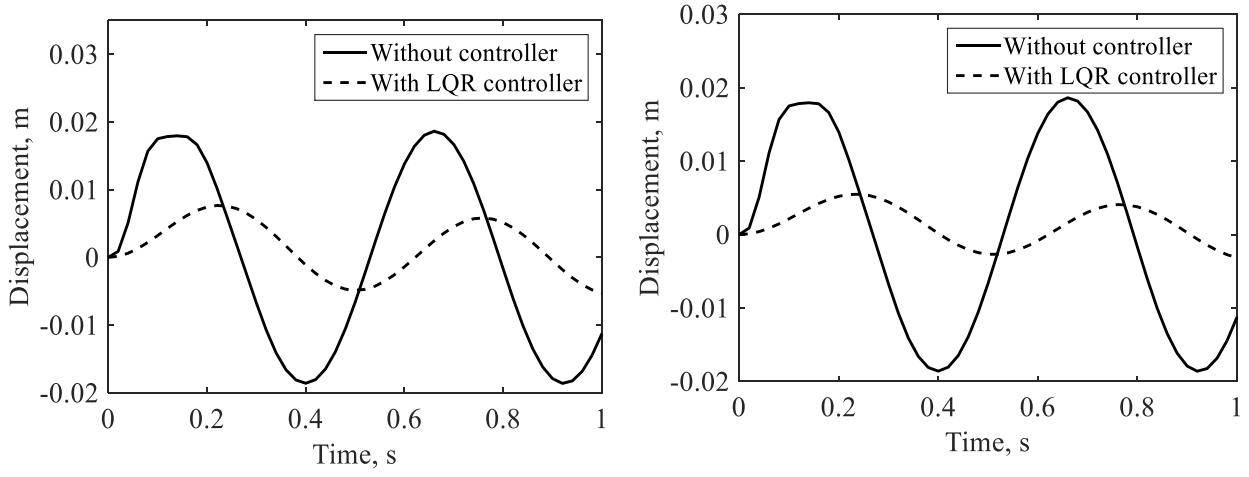

(a) (b)

Figure 4.1: Controlled flapping tip deflection for (a) $Q = 200I$ (b) $Q = 500I$

Figure 4.2 shows the lead-lag deflections of the rotor blade tip due to vibration, ranging from -0.003 to 0.003 m which is much smaller than the flapping case. The lead-lag deflections occur due to the drag force encountered by the rotor blade which is much smaller than the lift force. Also, the rigidity of the blade along the z-axis is significantly higher. The controlled deflections plotted in Fig. 4.2 (a) and Fig. 4.2 (b) show that the increase of the controller effort

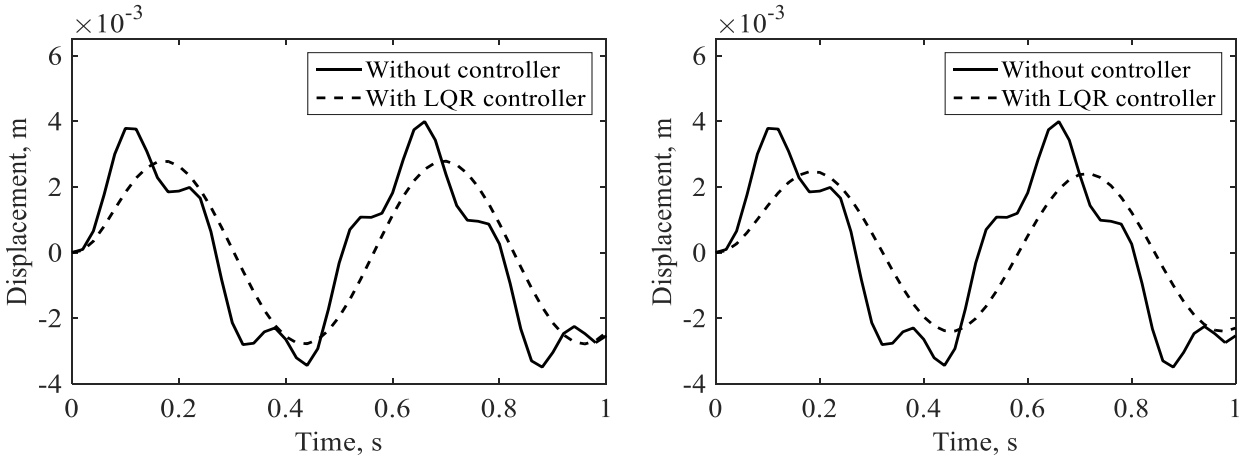

Figure 4.2: Controlled lead-lag tip deflection for (a) $Q = 200I$ (b) $Q = 500I$

does not have any visible effect on the deflections. Due to very small deflections, the effect of the controller effort is not noticeable.

Figure 4.3 shows the torsional deflections of the rotor blade tip due to the torsional moment produced by the aerodynamic moment. The torsional deflections ranges from -0.002 to 0.002 rad. The frequency in the torsional mode of vibration is significantly higher than the flapping and lead-lag cases. As the unit of deflections for the torsional deflections is rad, the value

is not comparable to the bending deflections. However, the generated deflections do not have any important contribution to the overall vibration.

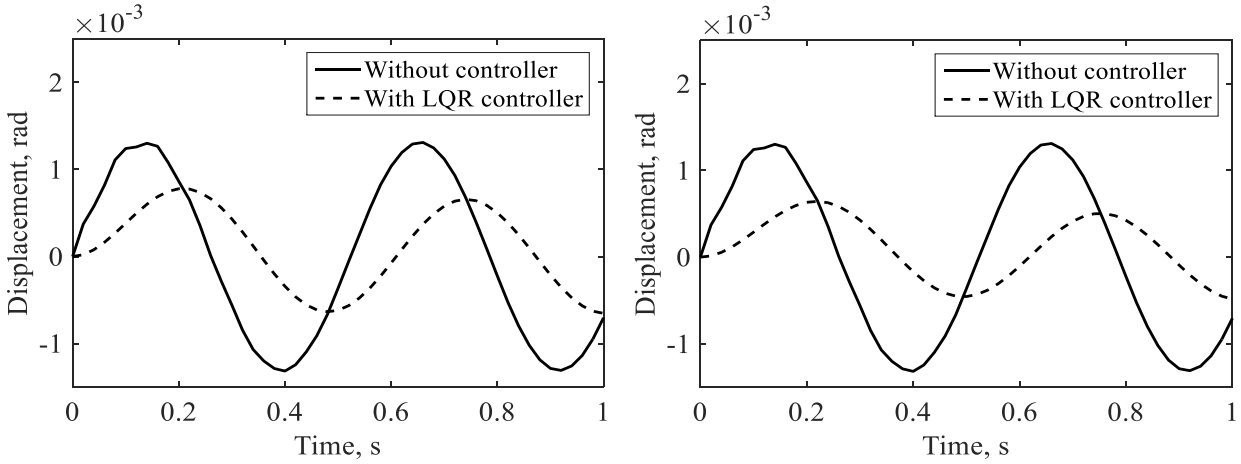

Figure 4.3: Controlled torsional tip deflection for (a) $Q = 12000I$ (b) $Q = 24000I$

Case 2: Step Excitation Load

Figures 4.4–4.6 show the response of the state-space model for the step excitation and the controlled deflections for the flapping, lead-lag, and torsional deflections for hovering.

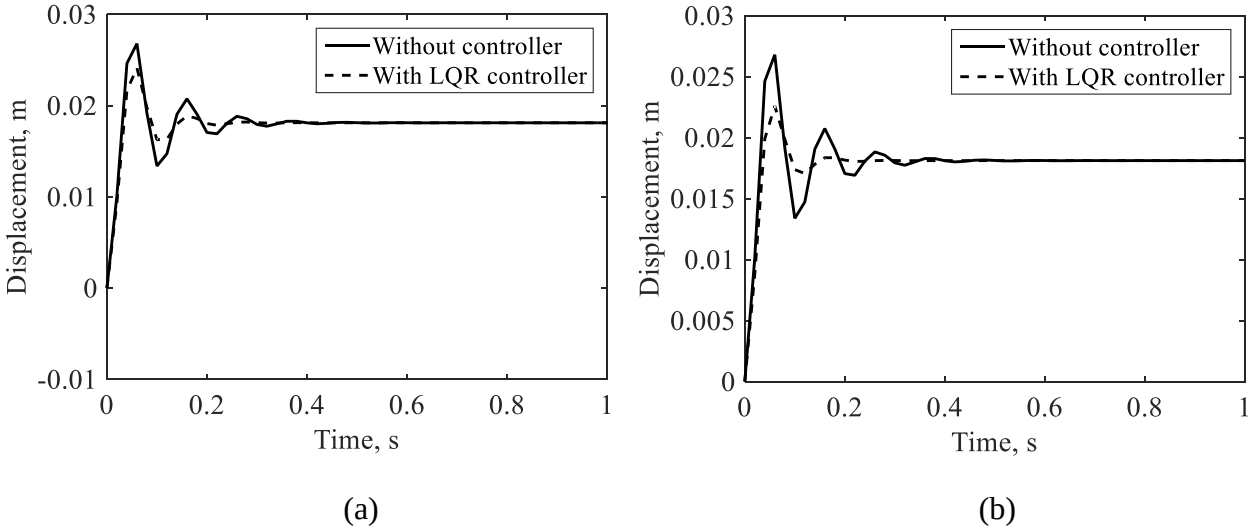

Figure 4.4: Controlled flapping tip deflection for (a) $Q = 0.2I$ (b) $Q = 0.4I$

The peak deflection for the step excitation is higher than the sinusoidal excitation for the flapping case. The similar phenomena are also observed for the lead-lag and torsional deflections cases as shown in Figs. 4.5 and 4.6.

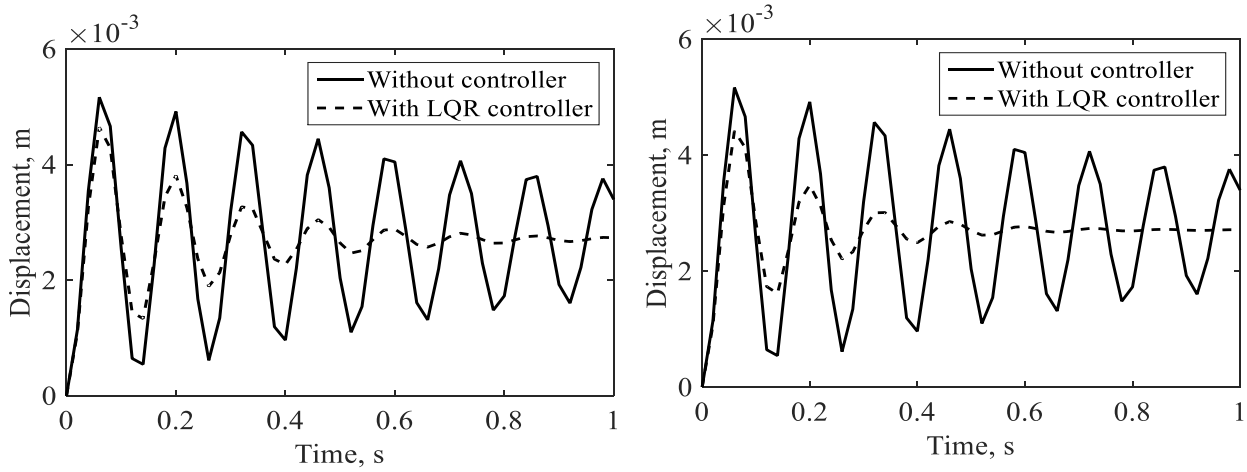

Figure 4.5: Controlled lead-lag tip deflection for (a) $Q = 2I$ (b) $Q = 4I$

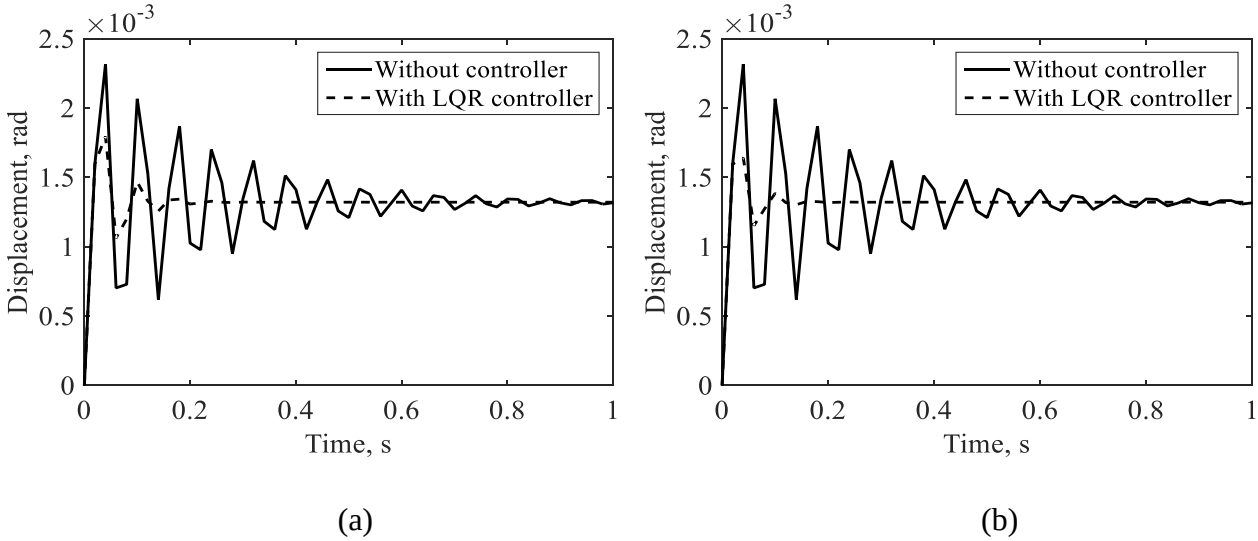

Figure 4.6: Controlled torsional tip deflection for (a) $Q = 0.4I$ (b) $Q = 0.8I$

4.3. Simulation Results for the Forward Flight

Case 1: Sinusoidal Excitation Load

In the forward flight, the blade velocity is different from the hovering flight as the helicopter velocity is added to the rotational velocity. The formulation of the lift, drag, and torsional moment for the forward flight are described in Chapter 2. Helicopter rotor blade experiences variable loads based on the helicopter speed which is, in general, represented by the advanced ratio. The analysis is performed for a fixed angle of attack, although the loads can vary with different angles of attack. The controlled deflections are obtained for advance ratios of 0.2 and 0.3, and the angle of attack of 4^o.

Figure 4.7 shows the flapping deflections at the blade tip for $\mu = 0.3$, ranging from -0.07 to 0.7 m. The flapping deflections are significantly higher than the hovering case due to the increased lift force. The controlled deflections are also shown for the weighting matrix $Q = 5I$ in

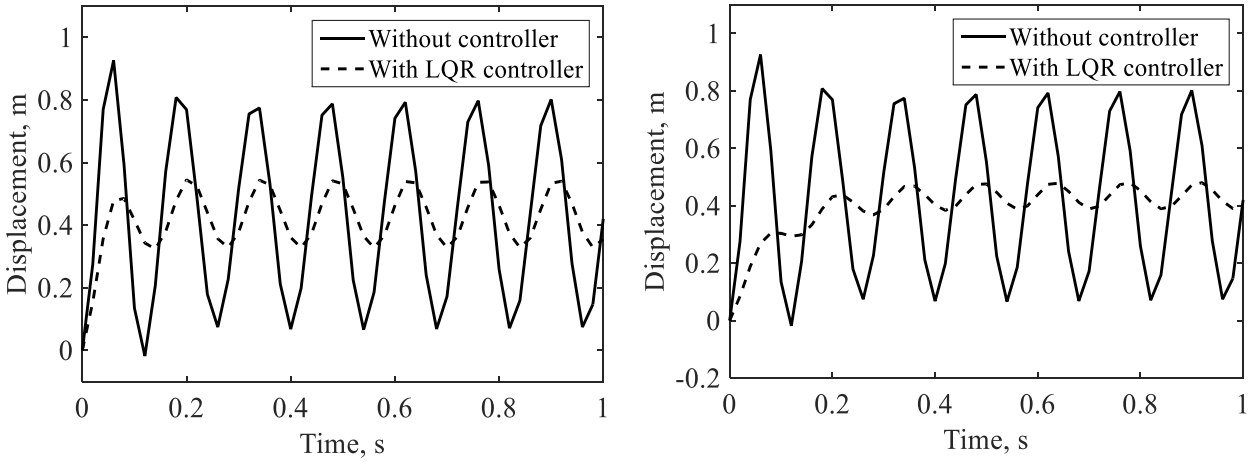

(a) (b)

Figure 4.7: Controlled flapping tip deflection for (a) $Q = 5I$ (b) $Q = 30I$

Fig. 4.7 (a) and $Q = 30I$ in Fig. 4.8 (b). The controlled deflections become smaller with the increase of the control effort.

Figure 4.8 shows the deflections and the controlled deflections for the lead-lag case ranging from -0.01 to 0.05 m. The controlled deflections are obtained for $Q = 600I$ in Fig. 4.8 (a) and $Q = 1200I$ in Fig. 4.8 (b). The increase of the controller effort has no significant effect on the controlled output.

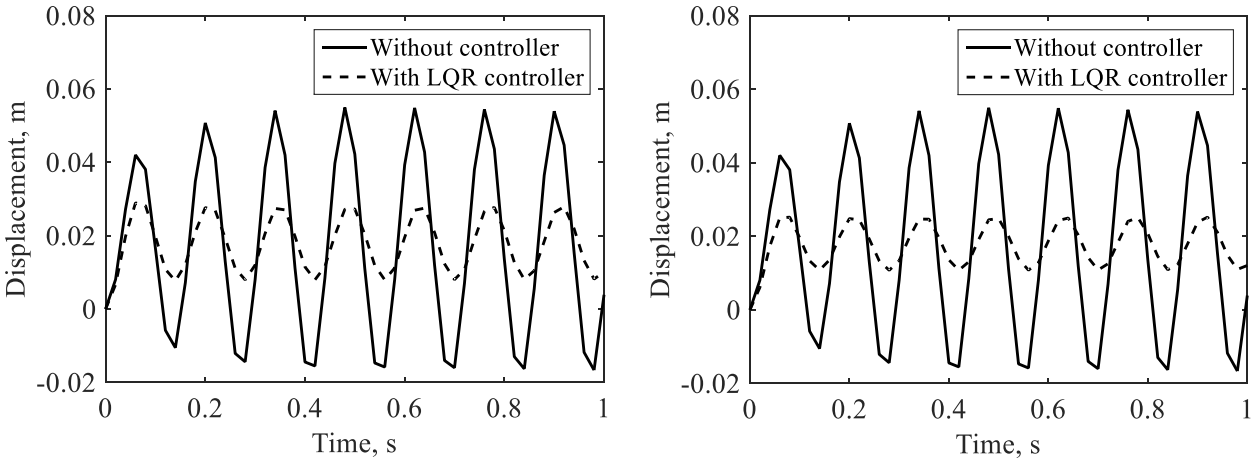

Figure 4.8: Controlled lead-lag tip deflection for (a) $Q = 600I$ (b) $Q = 1200I$

Figure 4.9 shows the blade tip deflections of the forward flight due to the torsional moment ranging from 0.02 to 0.05 rad which is also higher than the hovering case. Similar to the lead-lag case, the increase of the controller effort has less impact on the reduction of the deflections. Therefore, the controller effort should be kept minimum to attain the optimal torsional deflections during the forward flight.

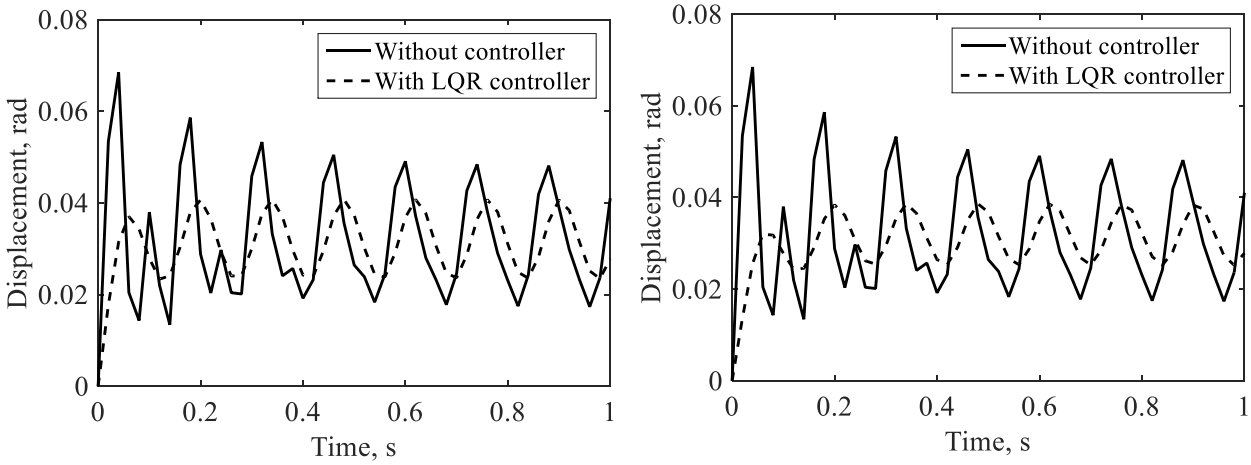

(a) (b)

Figure 4.9: Controlled torsional tip deflection for (a) $Q = 600I$ (b) $Q = 1200I$

Figures 4.10–4.12 show the deflections in flapping, lead-lag, and torsional case for $\mu = 0.2$, respectively. The deflections decrease with the decrease of the advance ratio.

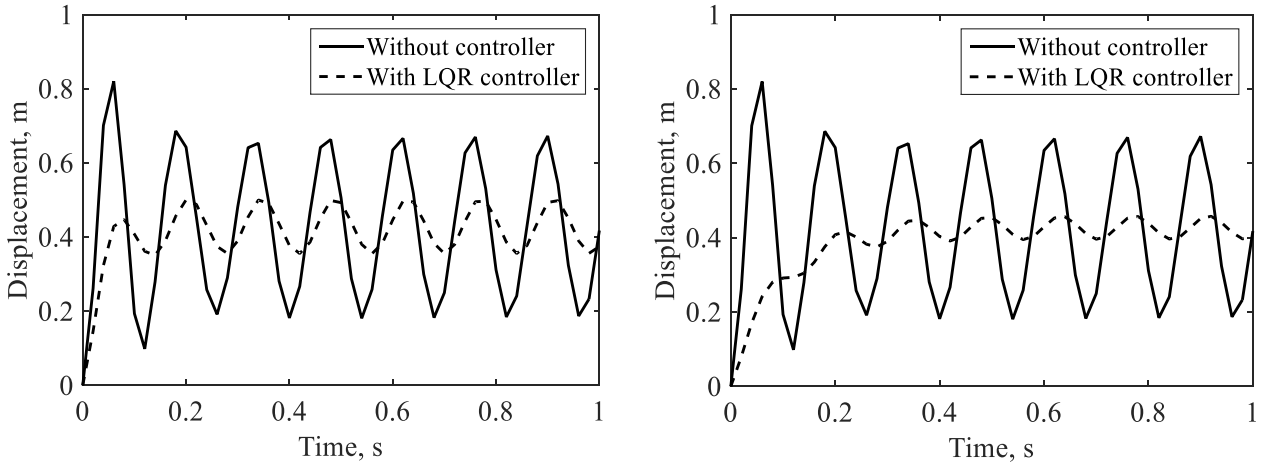

(a) (b)

Figure 4.10: Controlled flapping tip deflection for (a) $Q = 5I$ (b) $Q = 30I$ for $\mu = 0.2$

As a result, less controller effort is required to minimize the vibration. The controlled deflections are shown for two different Q values, mentioned in the corresponding captions for each case.

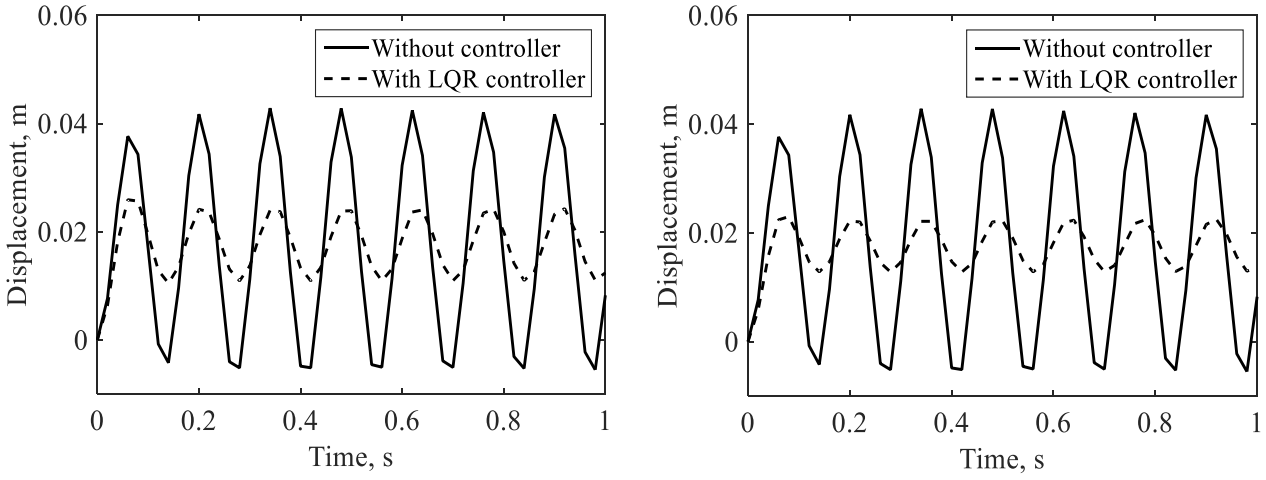

Figure 4.11: Controlled lead-lag tip deflection for (a) $Q = 600I$ (b) $Q = 1200I$ for $\mu = 0.2$

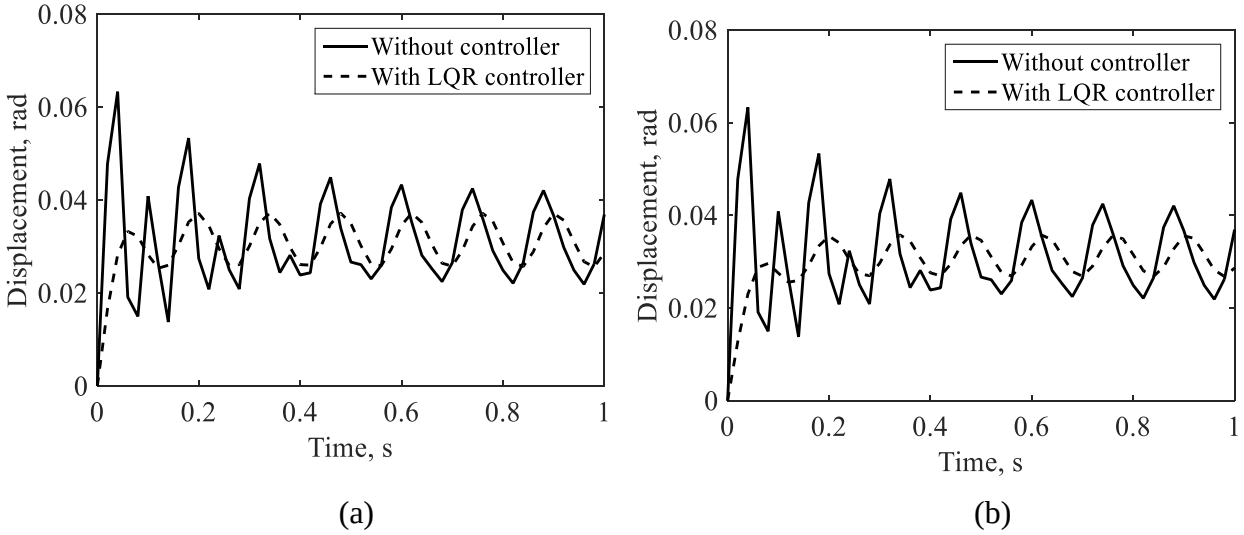

Figure 4.12: Controlled torsional tip deflection for (a) $Q = 600I$ (b) $Q = 1200I$ for $\mu = 0.2$

Case 2: Step Excitation Load

The state-space model is simulated using the step excitation force for all of the three degrees of vibration.

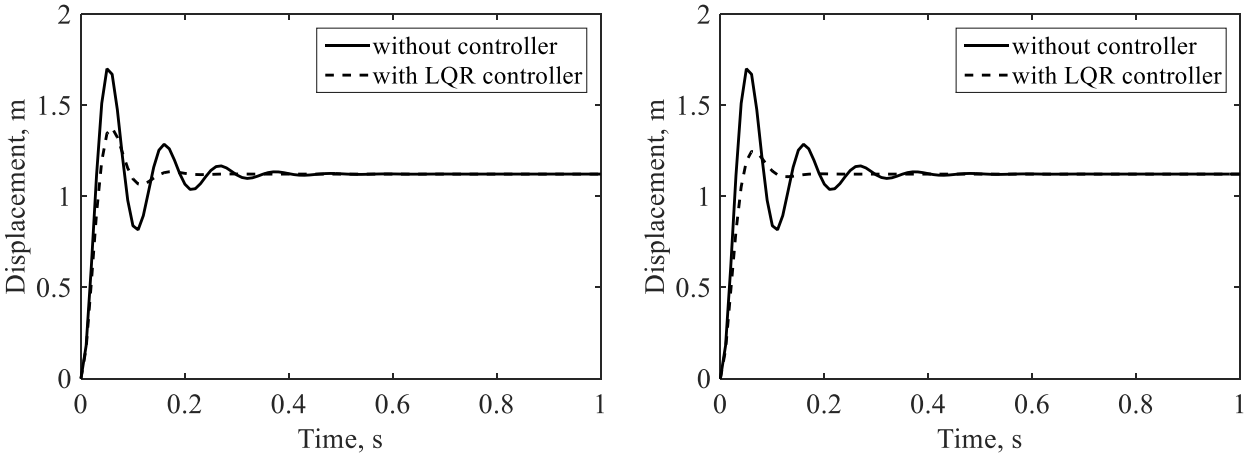

(a) (b)

Figure 4.13: Controlled flapping tip deflection for (a) $Q = 0.0005I$ (b) $Q = 0.001I$ for $\mu = 0.3$

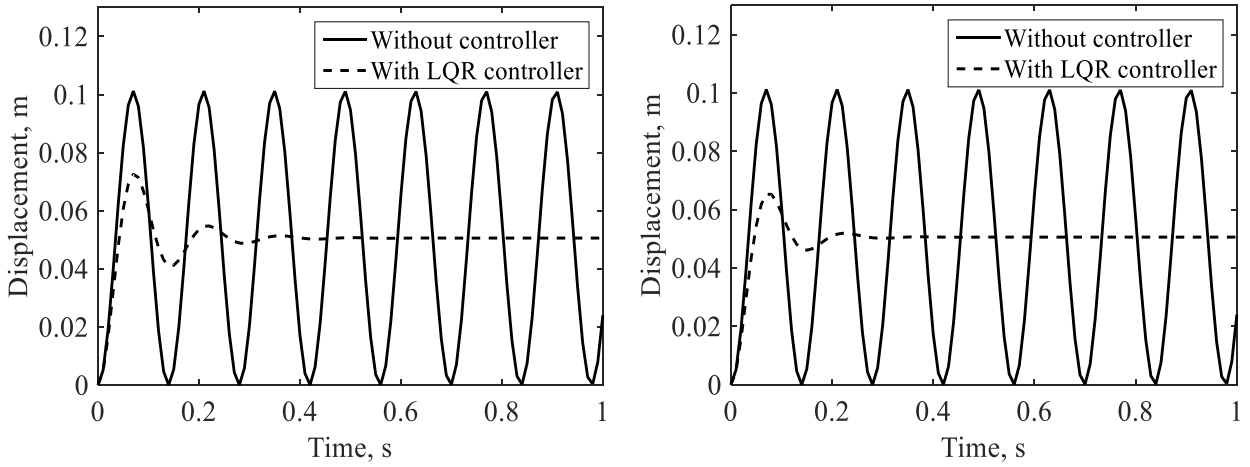

(a) (b)

Figure 4.14: Controlled lead-lag tip deflection for (a) $Q = 0.2I$ (b) $Q = 0.4I$ for $\mu = 0.3$

Figures 4.13–4.15 show the deflections of the blade tip due to step forces and the corresponding controlled deflections are also shown accordingly. The deflections due to step excitation forces are higher than those of the sinusoidal excitation forces for all of the cases. For the flapping deflections, the damping is much higher than other two cases due to the large aerodynamic damping. Hence, the vibration reduction is faster for the flapping deflections.

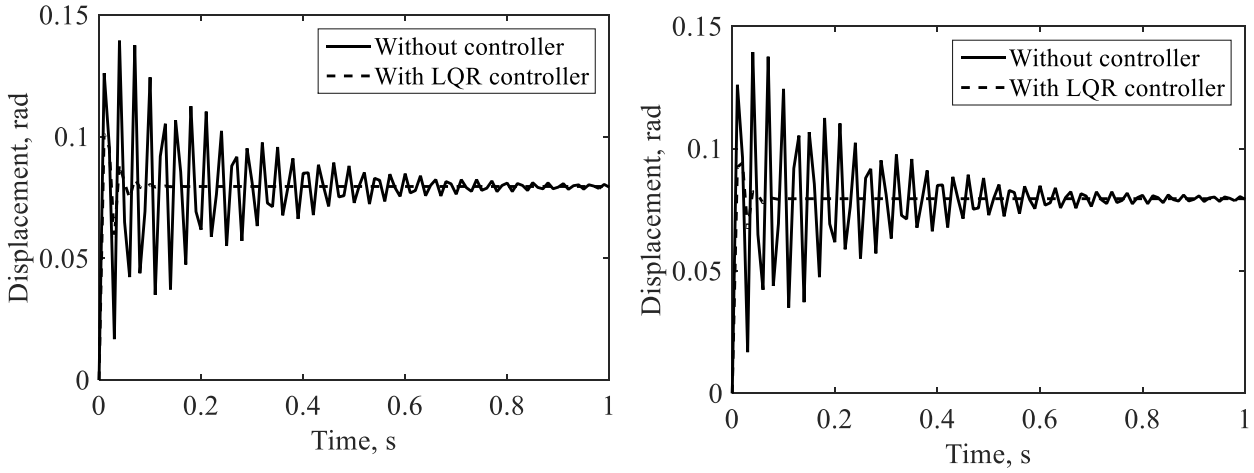

(a) (b)

Figure 4.15: Controlled torsional tip deflection for (a) $Q = 0.2I$ (b) $Q = 0.4I$ for $\mu = 0.3$

Figures 4.16–4.18 show the deflections at the blade tip due to the step excitation for the forward flight with $\mu = 0.2$. The deflections decrease with the decrease of μ, similar to the sinusoidal excitation. The increase of the controller effort does not influence the outcome significantly. Therefore, the control effort should be kept minimum to save the cost.

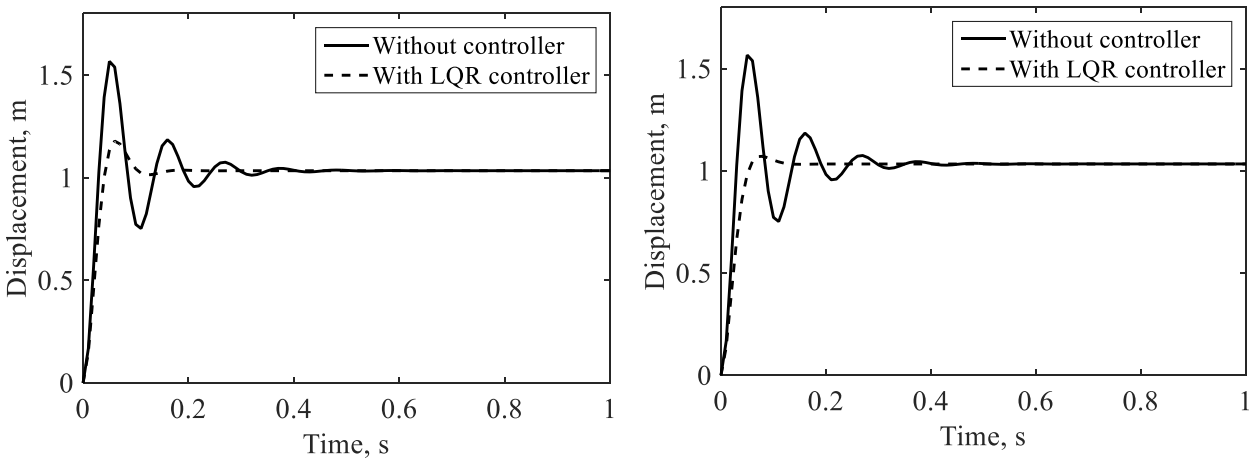

(a) (b)

Figure 4.16: Controlled flapping tip deflection for (a) $Q = 0.001I$ (b) $Q = 0.002I$ for $\mu = 0.2$

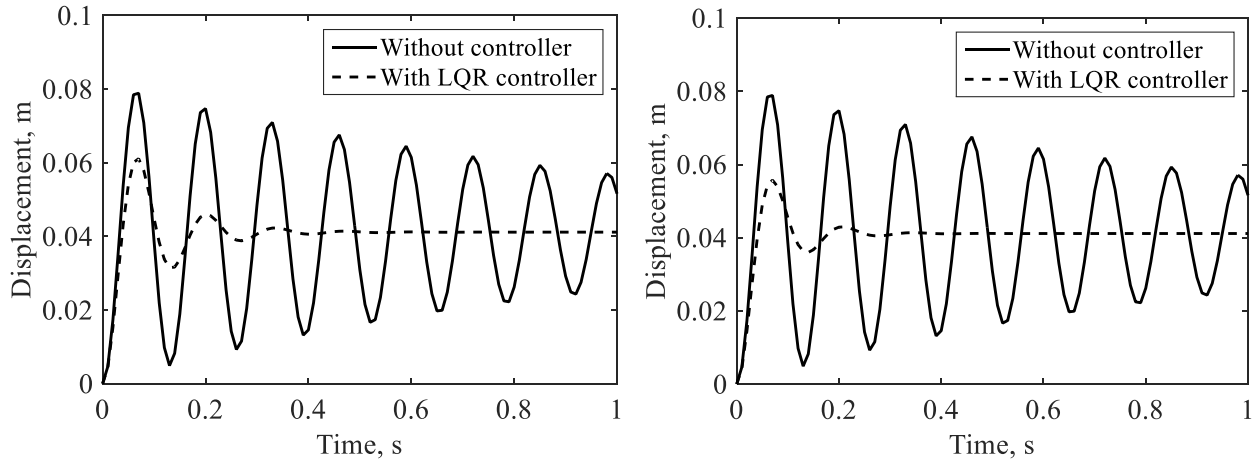

(a) (b)

Figure 4.17: Controlled lead-lag tip deflection for (a) $Q = 0.2I$ (b) $Q = 0.4I$ for $\mu = 0.2$

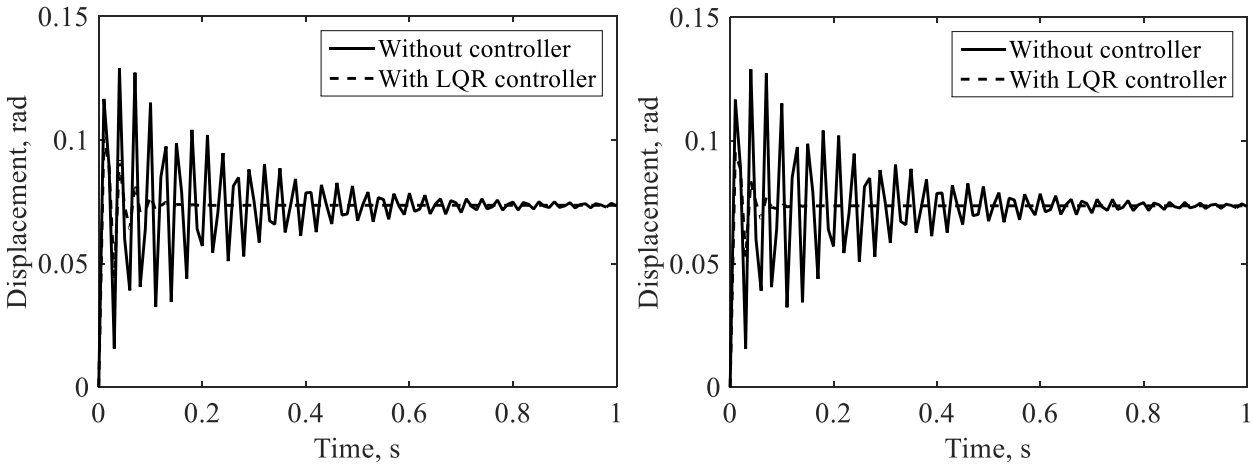

Figure 4.18: Controlled torsional tip deflection for (a) $Q = 0.001I$ (b) $Q = 0.002I$ for $\mu = 0.2$

Chapter 5

Conclusions and Recommendations

5.1 Concluding Remarks

In this thesis, the state-space model for an isolated rotor blade of Bo 105 is derived. The natural frequencies of the blade for the first mode of flapping, lead-lag, and torsional deflections are calculated by the modified Galerkin method. The analogy of the rotating cantilever beam is implemented to derive the three degrees-of-freedom vibration coupled equations of the blade for the hovering and the forward flight. The structure of the state-space model is applicable to construct the model of any rotating or nonrotating cantilever beam if the natural frequencies are known. Although only the first modes are considered for the modeling, the higher modes can be added to the state-space model by adding rows and columns to the matrices by including the corresponding natural frequencies. For the hovering and the forward flight, two different state-space models are derived because of the different natures of the responsible lift, drag, and torsional moments.

The suitability of the optimal controller is explored based on the research works published in the literature. Optimal control is considered superior to the classical control method due to the guaranteed stability and few controller parameters. Finally, a linear quadratic regulator is designed using the MATLAB control system toolbox. The derived state-space model is utilized for the controller design by tuning the controller parameters. The optimal controller effort is investigated to get the desired vibration reduction. For the forward flight, the deflections are simulated for two

different advance ratios which show that the deflections increase with the increase of the velocity, hence, require more controller effort.

5.2 Recommendations

Several assumptions are made to maintain the simplicity of the rotor blade model and controller design in this thesis. For the better accuracy of the analysis, the following recommendations are provided that can preclude the necessity of some of the assumptions and improve the reliability of the results.

1. For the simplicity of the state-space model, only the aerodynamic lift, drag, and moment are considered in the model. Although these are the major forces experienced by the rotor blade, various types of unsteady forces act on the blade which are dependent on the different flight conditions. To incorporate these forces a disturbance state-space model can be included for better analysis.
2. In this thesis, only the first modes of the flapping, lead-lag, and torsion are considered due to their significant contributions to the overall vibration. For further analysis, higher modes of the three degrees-of-freedom vibrations can be included. In that case, the dimension of the state-space model is increased according to the number of the considered modes. The natural frequency for each mode need to be determined and added to the additional rows of the state matrix.
3. The rotor blade is assumed as the Euler-Bernoulli beam without any twist angle in the development of the mathematical model. However, helicopter rotor blade has certain twist angle that varies for different helicopter models. This twist angle can be considered for the analysis to obtain more accurate results.

4. During the forward flight, the aerodynamic forces and moments vary with the change of the angle attack. As the angle of attack is the function of the azimuth angle, the value of this angle changes in a cyclic pattern. The variation of the angle of attack can be incorporated for the state-space model of the forward flight which makes the matrices time-variant.
5. For the IBC control, the dynamics of the actuators play very important role in the controller design. The tuning of the actuators also depends on the loads experienced by the rotor blade during the flight. To simulate the realistic response of the controller, the flight test data for the specific helicopter model is necessary. Additionally, different types of actuators can be tested and compared to determine the suitable one.

References

[1] Alkhatib, R., and Golnaraghi, M. F, 2003, "Active structural vibration control: a review," *Shock and Vibration Digest*, **35**(5) 367.

[2] Pearson, J. T., Goodall, R. M., and Lyndon, I., 1994, "Active control of helicopter vibration," *Computing and Control Engineering Journal*, **5**(6) 277–284.

[3] Fan, F. H., and Hall, S. R., 2014, "Gain-scheduled higher harmonic control for full flight envelope vibration reduction," 70th Annual Forum of the American Helicopter Society, Montreal, Canada

[4] Mura, R., Esfahani, A. M. G., and Lovera, M., 2014, "Robust harmonic control for helicopter vibration attenuation," American Control Conference, Portland, OR, USA.

[5] Friedmann, P., 2014., "On-Blade control of rotor vibration, noise, and performance: Just around the corner," *Journal of the American Helicopter Society*, **59**(4) 1–37.

[6] Lovera, M., Colaneri, P., Malpica, C., and Celi, R., 2006, "Closed-loop aeromechanical stability of hingeless rotor," *Journal of guidance, control, and dynamics,* **29**(1) 179−189.

[7] Kessler, Ch., 2011, "Active rotor control for helicopters: motivation and survey on higher harmonic control," *CEAS Aeronaut Journal*, **1**(1−4) 3–22.

[8] Kessler, Ch., 2011, "Active rotor control for helicopters: individual blade control and swashplateless rotor designs," *CEAS Aeronaut Journal*, **1**(1−4) 23–54.

[9] Johnson, W., 1982, "Self-tuning regulators for multicyclic control of helicopter vibration," *NASA-TP-1996*.

[10] Shaw, J., and Nicholas A., 1981, "Active control of the helicopter rotor for vibration reduction," *Journal of the American Helicopter Society*, **26**(3) 32–39.

[11] Shaw, J., 1989, "Higher harmonic control: wind tunnel demonstration of fully effective vibratory hub force suppression," *Journal of the American Helicopter Society*, **34**(1) 14−25.

[12] Straub, F. K., and Byrns, E. V., Jr., 1986, "Application of higher harmonic blade feathering on the OH-6A helicopter for vibration reduction," *NASA-CR-4031, NAS 1.26:4031.*

[13] Polychroniadis, M., 1990, "Generalized higher harmonic control-ten years of aerospatiale experience," 16th European Rotorcraft Forum, Glasgow, Scotland.

[14] Hammond, C. E., 1983, "Wind tunnel results showing rotor vibratory loads reduction using higher harmonic blade pitch," *Journal of the American Helicopter Society*, **28**(1) 10–15.

[15] Molusis, J. A., Hammond, C. E., and Cline, J. H., 1983, "A unified approach to the optimal design of adaptive and gain scheduled controllers to achieve minimum helicopter rotor vibration," *Journal of the American Helicopter Society*, **28**(2) 9–18.

[16] Nygren, K. P., and Schrage, D. P., 1989, "Fixed-gain versus adaptive higher harmonic control simulation," *Journal of the American Helicopter Society*, **34**(3) 51–58.

[17] Jacklin, S. A., 1998, "Comparison of five system identification algorithms for rotorcraft higher harmonic control," *NASA/TP-1998-207687*.

[18] Hall, S. R., and Wereley, N. M., 1993, "Performance of higher harmonic control algorithms for helicopter vibration reduction," *Journal of guidance, control, and dynamics*, **16**(4) 793–797.

[19] Patt, D., Liu, L., Chandrasekar, J., Bernstein, D. S., and Friedmann, P. P., 2005, "Higher-harmonic-control algorithm for helicopter vibration reduction revisited," *Journal of Guidance, Control, and Dynamics*, **28**(5) 918–930.

[20] Mura, R., 2015, "Rotorcraft vibration control: Adaptive vs LPV methods," *IFAC-Papers Online*, **48**(26), 109–114.

[21] Ham, N. D., 1980, "A simple system for helicopter individual blade control using modal decomposition.," Vertica, **4**(1) 23–28.

[22] Ham, N. D., 1980, "A simple system for helicopter individual blade control and its application to gust alleviation," 6th European Rotorcraft Forum, Bristol, England.

[23] Ham, N. D., Behal, B. L., and McKillip, R. M., 1983, "Helicopter rotor lag damping augmentation through individual-blade-control," *Vertica*, **7**(4) 361–371.

[24] Kessler, C., and Reichert, G., 1998, "Active control to augment rotor lead-lag damping," *Aeronaut Journal*, **102**(1011) 245–258.

[25] Richter, P., and Blaas, A., 1993, "Full scale wind tunnel investigation of an Individual Blade Control," 19th European Rotorcraft Forum, Cernobbio, Italy.

[26] Millot, T. A., and Friedmann, P. P., 1992, "Vibration reduction in helicopter rotors using an active control surface located on the blade," 33rd Structures, Structural Dynamics, and Materials Conference, Dallas, TX, USA.

[27] Roth., D., 2004, "Advanced vibration reduction by IBC technology", 30th European Rotorcraft Forum, Marseilles, France.

[28] Jacklin, S. A., Swanson, S., Blaas, A., Richter, P., and Teves, D., 2003, "Investigation of a helicopter individual blade control (IBC) system in two full scale wind tunnel tests," *NASA TP-2003–2122767*.

[29] Kessler, C., Fuerst, D., and Arnold, U. T. P., 2003, "Open-loop flight test results and closed-loop status of the IBC system on the CH-53G helicopter," 59th Annual Forum of the American Helicopter Society, Phoenix, AZ, USA.

[30] Norman, T. R., Shinoda, P. M., Kitaplioglu, C., Jacklin, S. A., and Sheikman, A., 2002, "Low-speed wind tunnel investigation of a full scale UH-60 rotor system," 58th Annual Forum of the American Helicopter Society, Montreal, Canada.

[31] Jacklin, S. A., Haber, A., de Simone, G., Norman, T. R., Kitaplioglu, C., and Shinoda, P. M., 2002, "Full-scale wind tunnel test of an individual blade control system for a UH-60 helicopter," 58th Annual Forum of the American Helicopter Society, Montreal, Canada.

[32] Norman, T. R., Theodore C., Shinoda, P. M., Fuerst, D., Arnold, U. T.P., Makinen, S., Lorber, P., and O'Neill, J., 2009, "Full-scale wind tunnel test of a UH-60 individual blade control system for performance improvement and vibration, loads, and noise control," 65th Annual Forum of the American Helicopter Society, Grapevine, TX, USA.

[33] Wei, F. S., and Weisbrich, A. L., 1979, "Multicyclic controllable twist rotor data analysis," *NASA-CR-152251*.

[34] Liu, L., Friedmann, P. P., Kim, I., and Bernstein, D. S., 2008, "Rotor performance enhancement and vibration reduction in presence of dynamic stall using actively controlled flaps," *Journal of the American Helicopter Society*, **53**(4) 152–163.

[35] Depailler, G., and Friedmann, P. P., 2002, "Alleviation of rotor vibrations induced by dynamic stall using actively controlled flaps with free play," 28th European Rotorcraft Forum, Bristol, England.

[36] Dieterich, O., Enenkl, B., and Roth, D., 2006, "Trailing edge flaps for active rotor control: aeroelastic characteristics of the ADASYS rotor system," 62nd Annual Forum of the American Helicopter Society, Phoenix, AZ, USA.

[37] Chopra, I., 1993, "Development of a smart rotor," 19th European Rotorcraft Forum, Cernobbio, Italy.

[38] Derham, R., Weems, D., Mathew, M. B., and Bussom, R., 2001, "The design evolution of an active materials rotor," 57th Annual Forum of the American Helicopter Society, Washington, DC, USA.

[39] Wilbur, M. L., Mirick, P. H., Yaeger, W. T. Jr., Langston, C.W. Cesnik, C.E.S., and Shin, S., 2001, "Vibration reduction testing of the NASA/ARMY/MIT active twist rotor," 57th Annual Forum of the American Helicopter Society, Washington, DC, USA.

[40] Monner, H. P., Opitz, S., Riemenschneider, J., and Wierach, P., 2008, "Evolution of active twist rotor design at DLR," AIAA/ASME/AHS Adaptive Structures Conference, Schaumburg, IL, USA.

[41] Opitz, S., Riemenschneider, J., and Monner, H. P., 2009, "Modal investigation of an active twist helicopter rotor blade," 20th International Conference on Adaptive Structures and Technologies, Hong Kong, China.

[42] Des Rochettes, H. M., Joly, D., Buchaniek, L., and Leconte P., 2009, "A new concept of active twist blade applied to main rotor of helicopter," RTO Applied Vehicle Technology Panel Symposium, Evora, Portugal.

[43] Thornburgh, R. P., Kreshock, A. R., Wilbur, M. L., Sekula, M. K., and Shen, J., 2014, "Continuous trailing-edge flaps for primary flight control of a helicopter main rotor," 20th Annual Forum of the American Helicopter Society, Montreal, Canada.

[44] Hoffmann, F., Keimer, R., and Riemenschneider, J., 2016, "Structural modeling and validation of an active twist model rotor blade," *CEAS Aeronautical Journal*, **7**(1) 43–55.

[45] Anobile, A., Bernardini, G., Gennaretti, M., and Testa, C., 2016, "Synthesis of active twist controller for rotor blade–vortex interaction noise alleviation," *Journal of Aircraft*, **53**(6) 1865–1874.

[46] Brillante, C., Morandini, M., and Mantegazza, P., 2016, "Periodic controllers for vibration reduction using actively twisted blades," *The Aeronautical Journal*, **120**(1233) 1763–1784.

[47] Peterson, R. L., 1995, "Full-scale hingeless rotor performance and loads," *NASA technical memorandum 110356*, Ames Research Center, CA, USA.

[48] Panda, B., and Chopra, I., 1986, "Dynamic stability of hingeless and bearingless rotors in forward," *Computers and Mathematics with Applications*, **12**(1) 111–130.

[49] Sarker, P., 2018, "Dynamic response of a hingeless helicopter rotor blade at hovering and forward flight," *PhD Dissertation*, University of New Orleans, LA, USA.

[50] Johnson, W., 1994, Helicopter Theory. New Jersey, Dover Publications.

[51] Abbott, I. H., Doenhoff, A. E. V., and Stivers, Jr., L. S., 1945, "Summary of airfoil data," NACA Report 824, Langley Memorial Aeronautical Laboratory, VA, USA.

[52] Dieterich, O., 1998, "Application of modern control technology for advanced IBC systems," 24th European Rotorcraft Forum, Marseilles, France.

[53] Gordon, L. J., 2000, "Principles of Helicopter Aerodynamics," *Cambridge Aerodynamic Series*.

Vita

The author was born in the city of Barisal, Bangladesh and passed his early school and college years in the same city. He obtained his Bachelor's degree in Mechanical Engineering in 2011 from the Islamic University of Technology, a subsidiary organ of OIC (Organization of Islamic Cooperation). After graduation, he joined the International Islamic University Chittagong and served there until September 2012 as a Lecturer in Mechanical Engineering. He completed his M.Sc. in Power Engineering from the Technical University of Munich, Germany in 2015. In the Summer 2016, he joined the University of New Orleans to pursue his Master's degree in Engineering with concentration in Mechanical Engineering and worked as a Graduate Assistant at the Department of Mechanical Engineering.